Cell Metabolism

Short article

Sphingomyelins in mosquito saliva reconfigure skin lipidome to promote viral protein levels and enhance transmission of flaviviruses

Graphical abstract

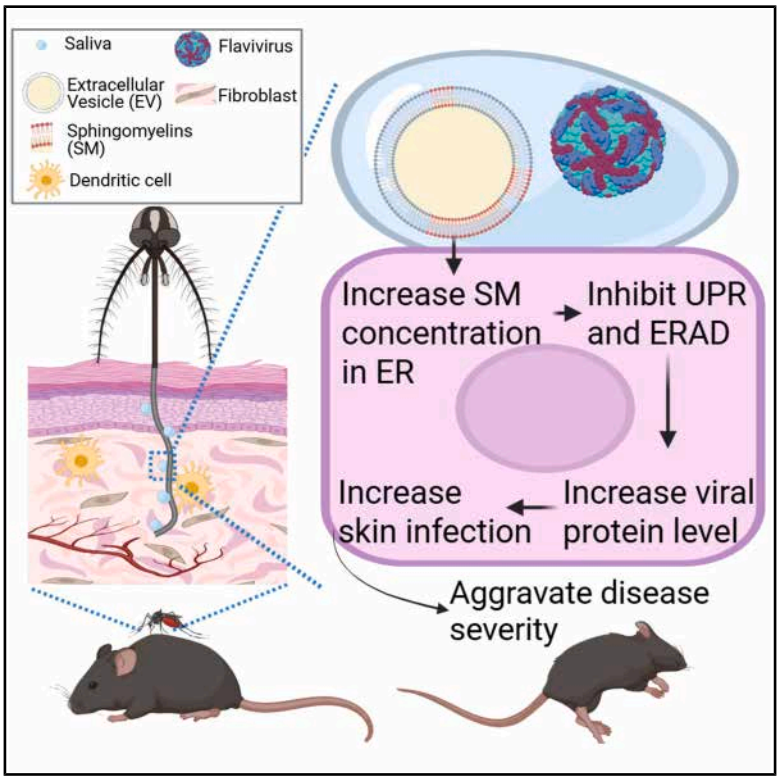

Highlights

- Mosquito salivary EV lipids enhance flavivirus infection in skin cells
- Mosquito EV lipids inhibit ERAD-mediated viral protein degradation
- Sphingomyelins within EVs increase ER sphingomyelin levels to enhance infection
- Salivary EV sphingomyelins enhance transmission and disease severity

Authors

Hacène Medkour, Lauryne Pruvost, Elliott F. Miot, ..., Dorothée Missé, Guillaume Marti, Julien Pompon

Correspondence

julien.pompon@ird.fr

In brief

Medkour et al. demonstrate that lipids of the sphingomyelin class in mosquito saliva facilitate the transmission of multiple flaviviruses. These salivary sphingomyelins reconfigure lipid homeostasis in skin cells, disrupting cellular mechanisms for viral protein degradation, thereby promoting skin infection at the bite site—a key determinant of transmission.

Medkour et al., 2025, Cell Metabolism *37*, 1601–1614
July 1, 2025
https://doi.org/10.1016/j.cmet.2025.05.015

CellPress

Cell Metabolism

CellPress
OPEN ACCESS

Short article

Sphingomyelins in mosquito saliva reconfigure skin lipidome to promote viral protein levels and enhance transmission of flaviviruses

Hacène Medkour,[1] Lauryne Pruvost,[1] Elliott F. Miot,[1] Xiaoqian Gong,[2] Virginie Vaissayre,[3] Mihra Tavadia,[1] Pascal Boutinaud,[1] Justine Revel,[1] Atitaya Hitakarun,[4] Wannapa Sornjai,[4] Jim Zoladek,[5] Duncan R. Smith,[4] Sébastien Nisole,[5] Esther Nolte-'t Hoen,[2] Justine Bertrand-Michel,[6,7] Dorothée Missé,[1] Guillaume Marti,[7,8] and Julien Pompon[1,4,9,*]

[1]MIVEGEC, University Montpellier, IRD, CNRS, Montpellier, France
[2]Department of Biomolecular Health Sciences, Faculty of Veterinary Medicine, Utrecht University, Utrecht, the Netherlands
[3]DIADE, University Montpellier, CIRAD, IRD, Montpellier, France
[4]Institute of Molecular Biosciences, Mahidol University, Nakhon Pathom, Thailand
[5]Institut de Recherche en Infectiologie de Montpellier (IRIM), University Montpellier, CNRS, Montpellier, France
[6]I2MC, Université de Toulouse, Inserm, Université Toulouse III – Paul Sabatier (UPS), Toulouse, France
[7]MetaboHUB-MetaToul, National Infrastructure of Metabolomics and Fluxomics, Toulouse, France
[8]Laboratoire de Recherche en Sciences Végétales, Metatoul-AgromiX Platform, Université de Toulouse, CNRS, INP, 24 Chemin de Borde Rouge, Auzeville, Auzeville-Tolosane 31320, France
[9]Lead contact
*Correspondence: julien.pompon@ird.fr
https://doi.org/10.1016/j.cmet.2025.05.015

SUMMARY

Many flaviviruses with high pandemic potential are transmitted through mosquito bites. While mosquito saliva is essential for transmission and represents a promising pan-flaviviral target, there is a dearth of knowledge on salivary metabolic transmission enhancers. Here, we show that extracellular vesicle (EV)-derived sphingomyelins in mosquito saliva reconfigure the human cell lipidome to increase viral protein levels, boosting skin infection and enhancing transmission for flaviviruses. Lipids within internalized mosquito EVs enhance infection in fibroblast and immune human primary cells for multiple flaviviruses. Mosquito EV lipids selectively increase viral translation by inhibiting infection-induced endoplasmic reticulum (ER)-associated degradation of viral proteins. Infection enhancement solely results from the sphingomyelins within salivary mosquito EVs that augment human cell sphingomyelin concentration. Finally, EV-lipid co-inoculation exacerbates disease severity *in vivo* in mouse transmission assays. By discovering and elucidating how metabolic components of mosquito saliva promote transmission of flaviviruses, our study unveils lipids as a new category of targets against vectored transmission.

INTRODUCTION

Several flaviviruses that cumulatively infect half a billion people annually, causing more than 120,000 fatalities and $9 billion in economic loss, are transmitted within mosquito saliva during biting.[1] Nearly the entire human population is threatened by dengue virus (DENV), Zika virus (ZIKV), and West Nile virus (WNV), the most prevalent flaviviruses, due to the wide geographic distributions of their mosquito vectors.[2–5] Following an infectious bite, flaviviruses are deposited in the skin[6] and initially multiply in fibroblasts and myeloid cells before systemic infection.[7] Amplification in skin is shared among flaviviruses and is necessary for transmission, representing a promising target for much-needed pan-flaviviral interventions.[8–10] Multiple lines of evidence indicate that components in mosquito saliva enhance flavivirus infection[9,11,12] in human cells,[13–15] mouse models,[6,16–21] and non-human primates.[22] While several salivary proteins enhance bite-initiated skin infection,[10,12] human populations living in endemic areas develop immunogenic reactions[23,24] that can abrogate the transmission-enhancing capacity of salivary proteins,[25–27] therefore pointing to additional non-immunogenic transmission enhancers. Indeed, there is a total lack of data on mosquito salivary metabolic components and their function in transmission.

Flaviviruses are enveloped single-stranded positive-sense RNA viruses that rely on the host cell lipidome throughout their multiplication cycle.[28–32] Lipids from various classes have to be reconfigured to accommodate the flavivirus multiplication cycle. Of particular interest, sphingolipids are major structural lipids and were regulated in different human cells upon flavivirus infections[33–36] and in dengue patient sera.[37] Sphingolipids have a C_{18} sphingosine backbone with a polar headgroup that can be linked to a variety of molecules, producing a range of sphingolipids from the

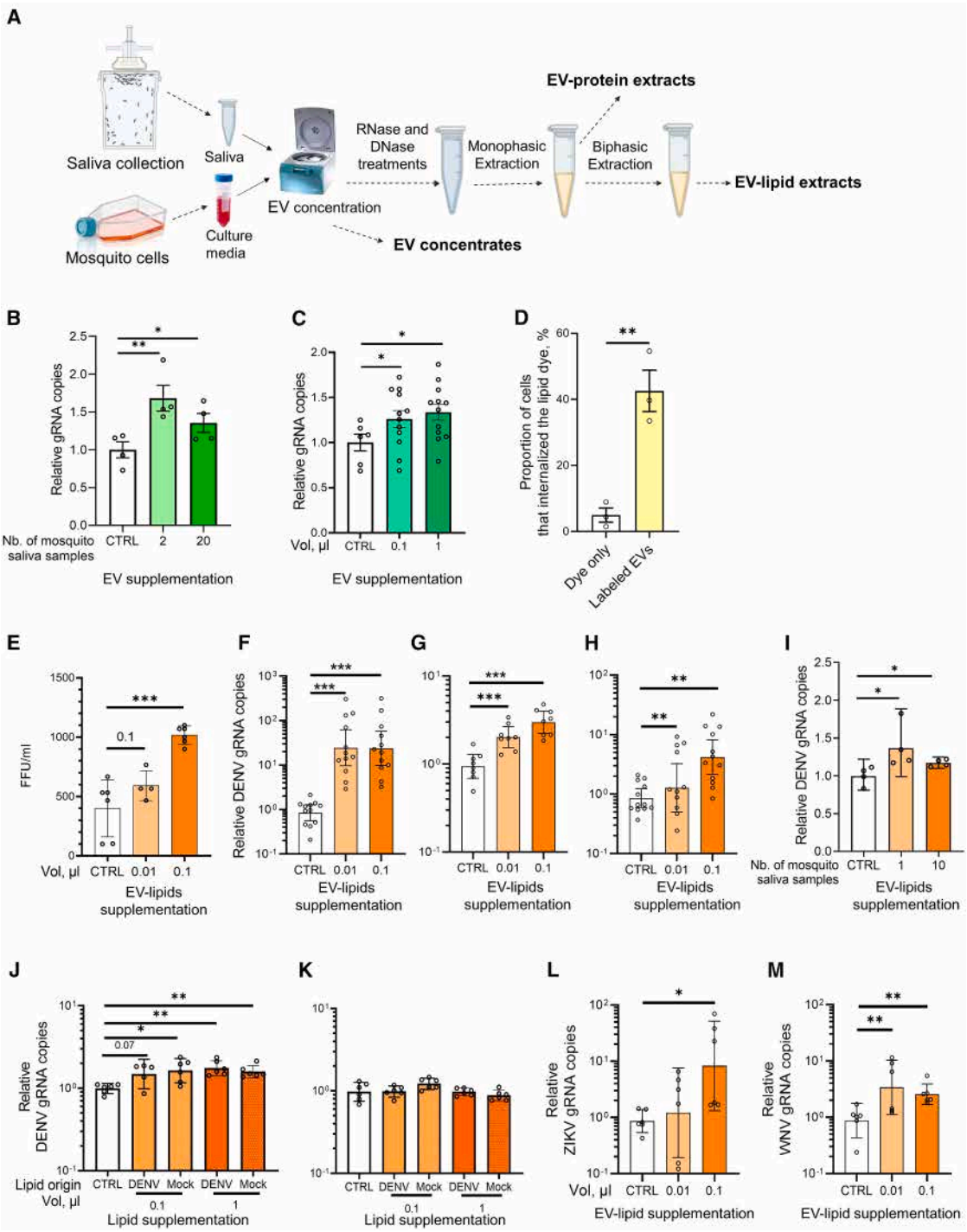

Figure 1. Lipids from mosquito EVs enhance flavivirus infection in multiple human cell types

(A) Protocol of isolation and extraction of EVs derived from mosquito saliva and cells.

(B and C) DENV gRNA in Huh7 supplemented with EV concentrates derived from saliva (B) and cells (C).

(D) Percentage of cells that internalized EVs derived from cells. Bars indicate mean ± SEM from 3 repeats.

(E–H) DENV FFU (E) and DENV gRNA (F) in Huh7, NHDF (G), and moDC (H) supplemented with EV lipids derived from cells. Extract LIP1.1 (Data S2B).

(I) DENV gRNA in Huh7 supplemented with EV lipids derived from saliva. Extract LIPSal (Data S2B).

(J and K) DENV gRNA in Huh7 supplemented with DENV-lipids from mosquito (J) or mammalian (K) cells. Mock indicates supplementation with lipids from the same density fraction from mock-infected cells. Lipid extracts detailed in Data S2C.

(legend continued on next page)

simplest ceramide to the more complex glycosphingolipids.[38] When linked to a phosphorylcholine group, ceramides produce sphingomyelins (SMs). SMs promote infection for WNV in fibroblasts and in mice,[39,40] and for Japanese encephalitis virus, another medically relevant flavivirus, in mouse cells.[41]

Here, we leveraged our recent discovery of extracellular vesicles (EVs) in mosquito saliva[42] to explore the function of salivary lipids in flavivirus transmission. EVs are spheroid structures delimited by a lipid bilayer membrane that act as cell-free intercellular delivery vehicles, transferring cargo and membrane components such as lipids into adjacent recipient cells.[43] We show that EV-derived SM lipids in mosquito saliva increase skin cell infection and the resulting transmission for multiple flaviviruses through reconfiguration of the human cell lipidome to inhibit endoplasmic reticulum (ER)-associated viral protein degradation. Thus, our study discovers and mechanistically elucidates the first metabolic transmission enhancer in vector-borne diseases.

RESULTS

Mosquito EV lipids enhance infection for flaviviruses in transmission-relevant human cells

To investigate the impact of salivary EVs, we collected hundreds of saliva by adapting a previous protocol,[44] concentrated EVs through ultracentrifugation (Figure 1A), supplemented permissive Huh7 cells with concentrated EVs during DENV infection, and quantified infection at 72 h post-infection (hpi). Supplementation with 2 or 20 saliva samples enhanced infection (Figure 1B), while cell survival was not affected (Figure S1A). We then repeated the experiments with EVs derived from a mosquito cell model (Figure 1A). Supplementation with 0.1 and 1 μL of cell EV concentrate increased infection as measured by intracellular DENV genomic RNA (gRNA) copies (Figure 1C) while not affecting cell viability (Figure S1C). Importantly, mosquito EVs were internalized by human cells as shown by the high proportion of cells that contained the lipid dye used to pre-label EVs (Figure 1D), strongly suggesting transfer of EV components inside the cells. To test the effect of EV proteins, we supplemented hepatocellular carcinoma cells with 0.051, 0.485, 0.51, or 4.85 μg of EV-protein extracts, encompassing the amount of proteins supplemented through intact EVs. While cell survival was marginally reduced for the higher EV-protein quantities (Figure S1D), none of the EV-protein quantities altered DENV gRNA levels (Figure S1E). By contrast, supplementation with 0.01 or 0.1 μL of EV-lipid extract (Data S2B) increased DENV infectious particles in supernatant and intracellular DENV gRNA (Figures 1E and 1F) and did not alter cell survival (Figure S1F). To assess the impact of mosquito EV lipids on cell types relevant to transmission, we infected primary skin dermal fibroblasts and monocyte-derived dendritic cells (moDCs) upon mosquito EV-lipid supplementation. In both primary cell types, DENV infection increased (Figures 1G and 1H), while cell viability was not affected (Figures S1G and S1H). To validate the cell model and assess the function of salivary EV lipids, we extracted EV lipids from mosquito saliva (Figure 1A). As for cell-derived EVs, supplementation with salivary EV lipids enhanced DENV infection (Figures 1I and S1B). These results reveal that lipids contained in mosquito EVs enhance DENV infection in multiple transmission-relevant cell types.

DENV envelope contains lipids, whose composition partially varies when viruses derive from mosquito or mammalian cells.[45,46] To evaluate whether the virion lipids similarly increased infection, we produced DENV in mosquito and monkey cells and isolated virions from EVs[47] using discontinuous sucrose density gradient. The purified DENV samples were obtained from our previously published study,[46] and we confirmed DENV isolation by detecting a high quantity of DENV gRNA (Data S2C). We extracted lipids from the DENV density fractions and, as controls, extracted lipids from the same density fraction from mock-infected cells (Data S2C). Lipid extracts either from DENV produced in mosquito cells or control mock-infected cells increased infection (Figure 1J), indicating that the enhanced infection resulted from lipids in mock samples. Based on partially overlapping density between DENV and EVs,[47,48] we reasoned that the DENV density fractions also contained EVs. By contrast, supplementation with either DENV or mock-infected lipids from mammalian cells did not alter DENV infection (Figure 1K). Cell viability was unaffected in all conditions (Figures S1I and S1J). These results suggest that virion lipids do not influence infection.

Finally, we observed an increased infection for both WNV and ZIKV (Figures 1L, 1M, S1K, and S1L). Contrarily, replication of chikungunya virus (CHIKV), the most prevalent mosquito-borne alphavirus,[49] was not affected (Figures S1M and S1N). Altogether, our results reveal that lipids within internalized mosquito EVs enhance infection for multiple flaviviruses in multiple transmission-relevant primary cell types.

Mosquito EV lipids selectively promote viral protein levels by dampening ER-associated degradation of viral proteins

To assess how mosquito EV lipids increase flaviviral infections, we determined the impact of mosquito EV-lipid supplementation on each stage of the DENV cellular cycle. At the onset of infection, attachment and internalization were not affected (Figures 2A and 2B). By contrast, translation of the incoming viral genomes, as estimated by viral protein quantity from 3 to 6 hpi, was progressively enhanced until a significant increase at 6 hpi (Figure 2C). Replication was then estimated as the kinetics of antigenome ((−)gRNA) production from 1 to 24 hpi. While (−)gRNA was not detected at 1 hpi as expected at the onset of the cycle, (−)gRNA was detected from 3 hpi onward, but its levels were not increased by mosquito EV lipids until 24 hpi (Figure 2D). This later increase is coherent with an enhanced replication resulting from higher quantities of viral proteins.[30] Finally, virion assembly and excretion were evaluated by quantifying infectivity of secreted particles as the ratio of (+)gRNA:FFU (FFU, focus-forming unit) in supernatant. Although mosquito EV

(L and M) ZIKV (L) and WNV (M) gRNA in Huh7 supplemented with EV lipids derived from cells. Extract LIP2.2 (Data S2B).
(B), (C), and (E)–(M) Geometric means ± 95% confidence interval (CI) from at least 4–6 replicates, indicated as points. FFU, focus-forming unit. *$p < 0.05$; **$p < 0.01$; ***$p < 0.001$ by t test.
See also Figures S1A–S1N and Data S1, S2B, and S2C.

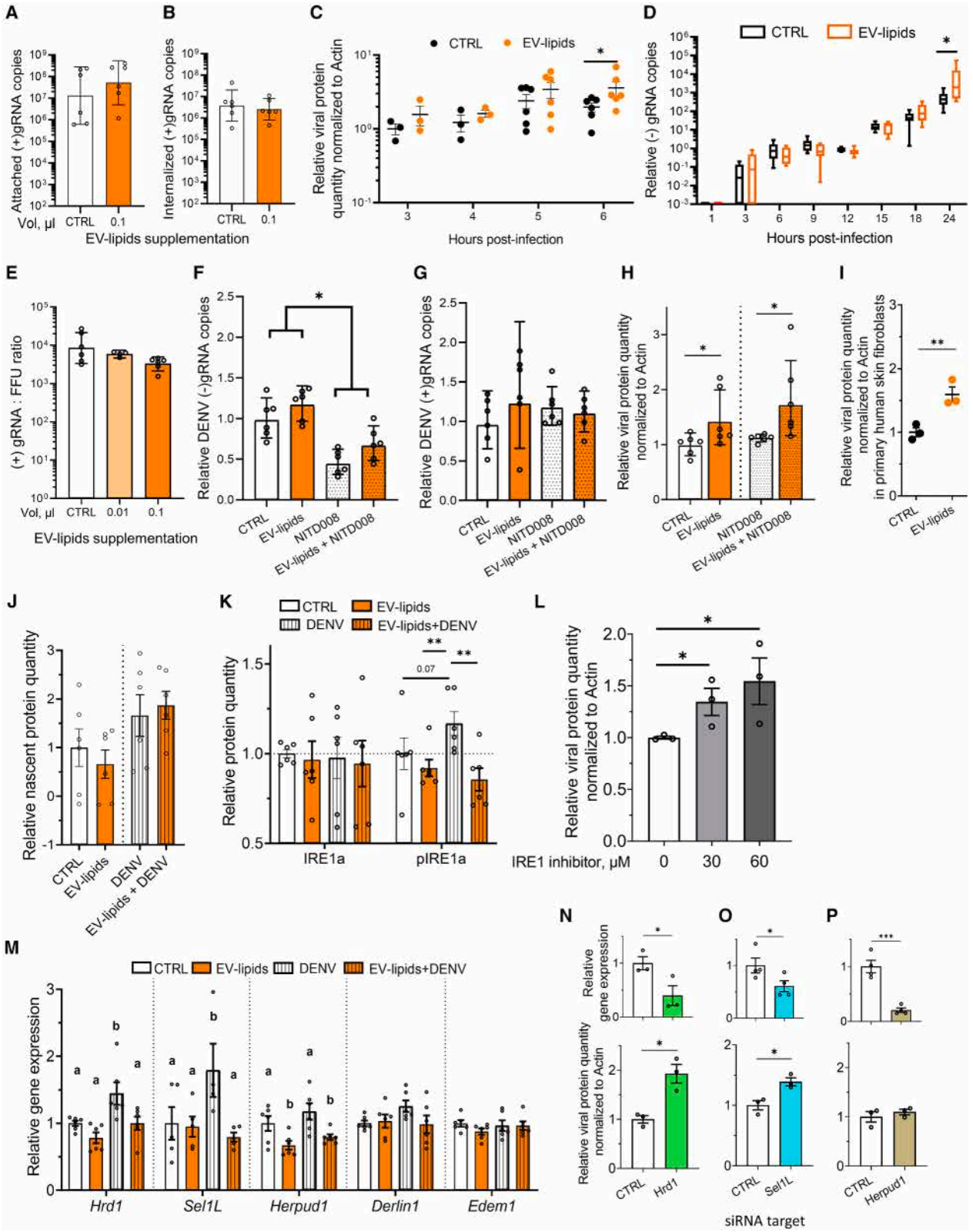

Figure 2. Mosquito EV lipids increase viral protein levels by altering ERAD of viral proteins

(A–E) DENV attachment (A), internalization (B), viral protein level (C), replication (D), and virion infectivity for Huh7 supplemented with EV lipids derived from cells. Extracts LIP1.1 and LIP2.2 (Data S2B).

(legend continued on next page)

lipids increased the production of infectious particles (Figure 1E), virion infectivity was not altered (Figure 2E). To confirm that mosquito EV lipids specifically promote viral translation, we inhibited viral replication with NITD008, a potent viral RNA synthesis inhibitor,[50] and quantified viral translation at 6 hpi. Upon NITD008 treatment with and without EV lipids, replication was reduced by 66% (Figure 2F), and incoming (+)gRNA quantities were not altered (Figure 2G), confirming replication inhibition and the lack of impact of EV lipids on internalization, respectively. However, the increase in viral protein levels by mosquito EV lipids was similarly maintained upon replication inhibition (Figure 2H). We confirmed the increased viral protein levels upon EV-lipid supplementation in primary skin fibroblasts (Figure 2I). Together, these results suggest that mosquito EV lipids specifically promote viral protein levels.

We then elucidated the mechanism by which EV lipids increase viral protein levels. First, we excluded any contributions of innate immunity by showing a lack of induced expression for interferon *(IFN)-β* and two IFN-stimulated genes (ISGs) (i.e., *MX1* and *CXCL10*) upon EV-lipid supplementation (Figures S1O–S1Q). Second, we showed that nascent protein quantity was not influenced by EV lipids alone and in combination with DENV (Figure 2J), as previously reported for DENV infection,[51,52] demonstrating that the EV-lipid effect was specific to viral proteins. Third, we tested whether the infection-induced unfolded-protein response (UPR)[53,54] was altered by EV lipids. While quantities of the signal activator inositol-requiring enzyme 1 (IRE1a)[55,56] were not altered by infection and EV lipids at 6 hpi (Figure 2K), the phosphorylated activating form (pIRE1a) was increased by DENV infection (Figure 2K), confirming the marginal induction of the UPR upon flavivirus infection.[52,57,58] Strikingly, EV-lipid supplementation prevented the infection-triggered increase in pIRE1a (Figure 2K). Chemical inhibition of IRE1a-mediated UPR activation elevated viral protein quantities at 6 hpi (Figure 2L), identifying a role for the UPR in reducing viral protein levels. Fourth, the UPR induces the ER-associated degradation (ERAD), which restores ER homeostasis by transporting misfolded proteins to the proteasome for degradation.[59,60] ERAD activation results in transcription of multiple genes, such as *Hrd1*, *Sel1L*, *Herpud1*, *Derlin1*, and *Edem1*.[61] By quantifying how EV lipids and DENV infection influenced their expressions, we observed 3 groups of regulation patterns: *Hrd1* and *Sel1L* were induced by DENV infection, and their infection-induced activation was inhibited by EV lipids; *Herpud1* was not induced by infection but downregulated by EV lipids alone or in combination with infection; and *Derlin1* and *Edem1* were regulated neither by EV lipids nor infection (Figure 2M). Silencing of *Hrd1* and *Sel1L* but not *Herpud1* increased viral protein levels at 6 hpi (Figures 2N–2P), demonstrating the impact of ERAD on viral protein levels. Altogether, our results indicate that EV lipids dampen infection-induced UPR, blocking ERAD-mediated protein degradation, thereby enhancing viral protein levels.

SMs within mosquito salivary EVs increase SM concentrations in human cells to enhance infection

To identify the lipid class responsible for the infection enhancement, we first used targeted lipidomics to quantify 107 sphingolipids, phospholipids, neutral lipids, and fatty acids in EVs and reveal the presence of at least 11 sphingolipids (Figure 3A; Data S3A). Although EV-lipid composition varies with cell types, the first description of mosquito EV lipids broadly corresponds to lipid composition for mammalian EVs.[62] Second, we fractionated mosquito EV lipids using solid-phase extraction (SPE) columns (Figure 3B), producing 6 fractions and their corresponding controls (CTRL), obtained by eluting an empty SPE column with the same solvents. Upon supplementation with the different lipid fractions, only fraction 6 increased DENV infection at 72 hpi (Figure 3C), while cell viability was not altered in any conditions (Figures S2A and S2B). Using untargeted global lipidomics on all 6 fractions,[63] we detected 228 lipid species (Data S3B) and observed that fraction 6 was enriched in SM, containing 95% of all fractions SM (Figure 3D; Data S3B). Third, we showed that supplementing human cells with commercially purified SMs increased DENV infection (Figure 3E), as for WNV,[40] and viral protein levels (Figure 3F), as EV lipids (Figure 2). Furthermore, pre-treatment of the SM solution, fraction 6, and extracted EV lipids with sphingomyelinase (SMase) (Figure 3G) abrogated the infection increase (Figures 3H–3J). Additionally, we exposed human cells to EV lipids pre-treated with ceramidase (CERase) to deplete another lipid class present in F6 (Figure S2C). The infection increase mediated by EV lipids was not altered by ceramide depletion (Figures S2D and S2E), confirming that SMs are solely responsible for the infection increase. To extrapolate our findings to real-world transmission, we quantified SMs in EVs from mosquito saliva (Figure 3K) and found that single saliva contained between 1.64 and 4.07 pmol of SMs (Figure 3L). In comparison, EVs from mosquito cells used to produce 0.1 μL of EV-lipid extracts contained between 1.19 and 1.60 pmol of SMs (Figure 3K). Altogether, these results demonstrate that SMs found in EVs from mosquito saliva enhance flavivirus infection.

To understand the metabolomic interactions responsible for the lipid-mediated infection enhancement, we applied global lipidomics to human cells exposed to either (1) mosquito EV lipids, (2) DENV, or (3) DENV with mosquito EV lipids. Control cells were

(F–H) DENV replication (F), internalization (G), and viral protein levels (H) in Huh7 treated with NITD008 and supplemented with EV lipids at 6 hpi. Extracts LIP2.5_2 and LIP2.5_3 (Data S2B).
(I) DENV viral protein levels in primary neonatal human dermal fibroblasts supplemented with EV lipids at 6 hpi. Extract LIP7.3 (Data S2B).
(J and K) Nascent protein quantity (J), IRE1a and pIRE1a proteins (J) in Huh7 infected with DENV and supplemented with EV lipids at 6 hpi. Extracts LIP7.1 (Data S2B).
(L) DENV viral protein levels in Huh7 treated with IRE1 inhibitor at 6 hpi.
(M) Expression of ERAD genes (i.e., *Hrd1*, *Sel1L*, *Herpud1*, *Derlin1*, and *Edem1*) in Huh7 infected with DENV and supplemented with EV lipids at 6 hpi. Extract LIP7.1 (Data S2B).
(N–P) Gene expressions and DENV viral protein levels upon siRNA-mediated depletion of *Hrd1* (N), *Sel1L* (O), and *Herpud1* (P).
(A)–(C) and (E)–(G) Geometric means ± 95% CI. (D) Tukey box and whiskers from six replicates. (H)–(P) Means ± SEM. (M) Different letters indicate significant differences by least significant difference (LSD)'s test. Points represent repeats. $^{*}p < 0.05$; $^{**}p < 0.01$; $^{***}p < 0.001$ by t test.
See also Figures S1O–S1Q and Data S1, S2B, and S2C.

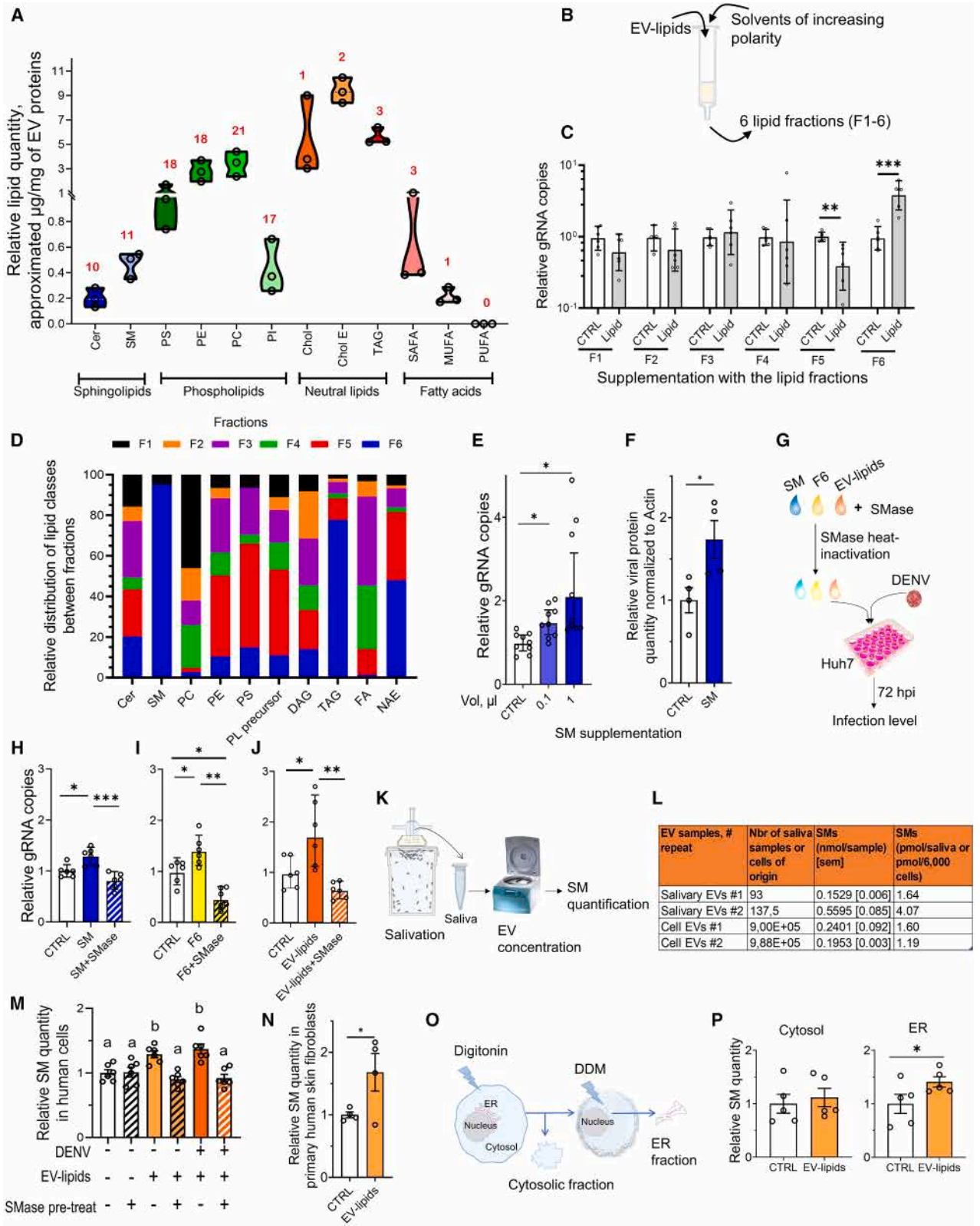

EV samples, # repeat	Nbr of saliva samples or cells of origin	SMs (nmol/sample) [sem]	SMs (pmol/saliva or pmol/6,000 cells)
Salivary EVs #1	93	0.1529 [0.006]	1.64
Salivary EVs #2	137,5	0.5595 [0.085]	4.07
Cell EVs #1	9,00E+05	0.2401 [0.092]	1.60
Cell EVs #2	9,88E+05	0.1953 [0.003]	1.19

Figure 3. SMs within mosquito salivary EVs are sufficient to enhance infection through SM concentration increase in human cell ER

(A) Cell-derived EV lipidome. Three biological replicates, represented by circles. Red numbers indicate detected species within lipid class.

(B) EV-lipid fractionation protocol.

(legend continued on next page)

exposed to neither of these. Cells were analyzed at 4 h post-treatment (hpt) to prevent an effect of the increased viral protein levels (Figure 2C). Among the 280 lipid species detected, 80 were significantly regulated in at least one condition (Figures S3A and S3B; Data S3C), revealing an early and complex lipidome modulation. To analyze the lipidome regulations, we clustered the regulated lipids, observing 9 regulation patterns (Figure S3A). To decode this complex dataset, we aligned with previous studies showing that flaviviruses modulate cellular lipidome for their benefits[64–66] and posited that infection-induced lipid regulation indicated a pro-viral environment. To facilitate interpretation, we normalized cluster trends to the control (Figure S3B).

Cluster 1 comprises nine lipids induced separately by infection and EV lipids and further upregulated during infection upon EV-lipid supplementation. Based on our postulate, lipids of cluster 1 were considered as pro-viral and associated with EV-mediated infection enhancement. Cluster 1 lipids included SMs, which promote WNV infection *in vivo*[39,40]; lysophospholipids, known to increase WNV genome replication[65]; phospholipids that influence DENV genome replication[64]; and short fatty acids. Lipids from clusters 2 and 4 were upregulated by infection. However, EV-lipid supplementation alone or combined with infection did not upregulate or amplify these lipids, suggesting that they were not associated with EV-mediated infection enhancement. Lipids from clusters 3 and 5–9 were downregulated by infection. While mosquito EV lipids alone similarly downregulated cluster 3 lipids, the infection-induced regulation was annihilated for infection upon EV-lipid supplementation. Cluster 5–7 lipids were upregulated by EV lipids, antagonizing the infection-induced regulations. By contrast, lipids from clusters 8 and 9 were downregulated by mosquito EV lipids as upon infection, potentially creating a pro-viral environment. Furthermore, infection combined with EV lipids amplified the downregulation of cluster 8 lipids and maintained the infection-induced reduction of cluster 9 lipids. Cluster 8 mostly comprised phospholipids (phosphatidylcholine [PC] and phosphatidylethanolamine [PE]), which are involved in membrane structure,[32] whereas cluster 9 lipids were mostly fatty acids (triacylglycerol [TAG] and diacylglycerol [DAG]), involved in energy metabolism.[67] Overall, EV lipids amplified the infection-induced concentration increase in certain lipids, including SMs (Figures S3A and S3B), potentially amplifying an infection-driven pro-viral environment.[64–66] To test whether the increased SM concentration in human cells was driven by EV-associated SMs, we exposed human cells to DENV and mosquito EV lipids, which had been depleted or not of SM by SMase pre-treatment (Figure 3G). At 4 hpt, exposition to heat-inactivated SMase alone did not alter SM cellular concentration, validating SMase inactivation (Figure 3M). While EV lipids alone and together with DENV increase SM cellular concentrations, SMase pre-treatment abrogated the increase in cellular SM concentration (Figure 3M). We confirmed that EV lipids increased intracellular SM concentrations in primary neonatal human dermal fibroblasts (Figure 3N). To better understand the cell compartment where the increased SM concentration takes place, we separately extracted the cytosol and ER (Figure 3O),[57] confirmed the fractionation by specifically detecting ER-associated Ribophorin I in the ER fraction and actin in the cytosolic fraction (Figure S3C), and observed that EV-lipid supplementation specifically increased SM concentration in the ER fraction at 4 h post-exposure (Figure 3P). Altogether, these results demonstrate that SMs in EV lipids quickly reconfigure the host lipidome by increasing SM concentration in the ER, where IRE1a is located.[68]

Mosquito EV lipids and SMs aggravate disease severity in a mouse model of transmission

To evaluate the impact of mosquito EV lipids on transmission, we inoculated a wild-type mouse model susceptible to WNV infection[26] with a sub-lethal dose of WNV in combination with 0.1 or 1 μL of mosquito EV lipids (Figure 4A), covering the range of SM quantities present in one saliva (Figure 3K). Since wild-type mice are not susceptible to DENV infection, we used WNV as a flavivirus model, as its infection is similarly enhanced by EV lipids (Figure 1M). Control mice received either DMSO alone (no inf.) or the WNV inoculum mixed with the vehicle for EV lipids (CTRL). Inoculum volume was designedly small (i.e., 10 μL) and injected in the dermis to mimic bite delivery of saliva in skin. We validated infection by monitoring RNAemia (Figures S4A–S4C), which does not reflect disease severity.[69–71] While infected mice lost weight, as expected from WNV infection,[69–71] the weight reduction was significantly amplified when WNV was co-inoculated with EV lipids (Figure 4B). Symptoms evaluated according to a clinical score ranging from 0 to 5 (Data S1), considering key WNV symptoms in mice and where 5 corresponds to death,[72] appeared on day 3 and progressively

(C) DENV gRNA in Huh7 supplemented with cell EV lipids F1-6 or corresponding control (CTRL).
(D) Lipid class composition of the cell EV-lipid fractions.
(E and F) DENV gRNA (E) and viral protein levels (F) in Huh7 supplemented with SM.
(G) SMase pre-treatment protocol.
(H–J) DENV gRNA in Huh7 supplemented with SMase-treated SM (H), F6 (I), and cell EV lipids (J). Extract LIP2.5_3 (Data S2B).
(K) Protocol for SM quantification in salivary EVs.
(L) SM quantity in EVs derived from mosquito saliva and cells.
(M) SM concentration in Huh7 infected with DENV and supplemented with cell EV lipids after SMase pre-treatment at 4 h post-exposure. Different letters indicate statistical differences by LSD test. Extract LIP2.5_3 (Data S2B).
(N) SM concentration in primary neonatal human dermal fibroblasts supplemented with cell EV lipids at 4 h post-exposure. Extract LIP7.3 (Data S2B).
(O) Cytosol and ER fractionation protocol.
(P) SM concentration in cytosolic and ER fractions of Huh7 supplemented with cell EV lipids.
(A) and (D) Cer, ceramide; SM, sphingomyelin; PS, phosphatidylserine; PC, phosphatidylcholine; PE, phosphatidylethanolamine; PI, phosphatidylinositol; Chol, cholesterol; CholE, cholesterol esters; SAFA, saturated fatty acid; MUFA, monounsaturated fatty acid; PUFA, polyunsaturated fatty acid; TAG, triacylglyceride; DAG, diacylglyceride; FA, fatty acid; NAE, N-acylethanolamine.
(C) and (D) F1-6, SPE fractions 1–6.
(C), (E), and (H)–(J) Geometric means ± 95% CI (F), (M), (N), and (P) means ± SEM. Points represent repeats. $*p < 0.05$; $**p < 0.01$; $***p < 0.001$ by t test.
See also Figures S2 and S3 and Data S1, S2B, S2C, and S3.

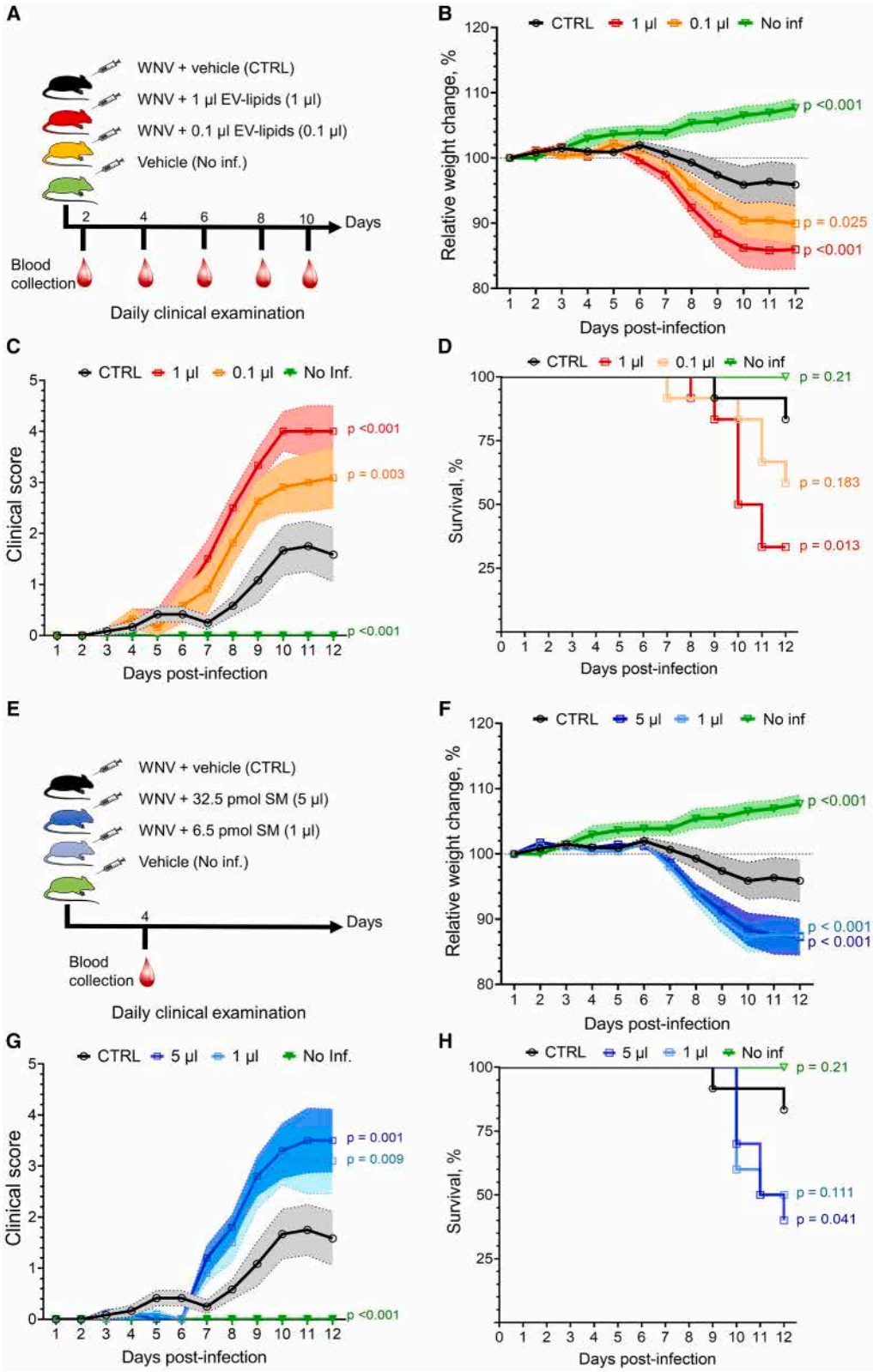

Figure 4. Intradermal co-inoculation of WNV with mosquito EV lipids or SMs increases disease severity in mice

(A) Experimental design for cell EV lipids co-inoculation. *n*, 12 per condition, 9 for no inf. Extracts LIP1.1 et LIP7.3 (Data S2B).

(B–D) Mean relative weight change ± SEM (B), mean clinical score ± SEM (C), and survival (D) over 12 days post injection.

(legend continued on next page)

aggravated until days 9–11 before plateauing or resorbing. As compared with mice solely injected with WNV, symptom severity increased with co-injection of 0.1 μL (mixed-effects ANOVA; interaction, $p = 0.003$) and 1 μL ($p < 0.001$) of EV lipids (Figure 4C). Similarly, while injection of WNV reduced survival to 83%, co-inoculation with 0.1 and 1 μL of EV lipids further diminished survival to 58 ($p = 0.183$) and 33% ($p = 0.013$), respectively (Figure 4D).

To determine whether SMs, responsible for the increased infection in cells (Figure 3), also enhance transmission, we co-inoculated 6.5 and 32.5 pmol of SMs with WNV in the mouse transmission model (Figure 4E). While SM co-inoculation did not alter RNAemia (Figure S4D), both doses reproduced key indicators of disease severity, including weight loss (Figure 4F), exacerbated symptoms (Figure 4G), and reduced survival (Figure 4H). Altogether, the *in vivo* infection assays mimicking bite-initiated transmission demonstrate that mosquito EV lipids, including SMs, amplify disease severity in a dose-dependent manner.

DISCUSSION

Our study demonstrates that SMs contained within mosquito salivary EVs enhance bite-initiated skin infection and the resulting transmission for flaviviruses by modulating the human cell lipidome, thereby increasing flaviviral protein levels by dampening viral protein degradation.

Our findings demonstrate that mosquito EV lipids mitigate infection-induced UPR-driven ERAD, impairing its antiviral function. Prior studies and the current one reported the activation of UPR by flavivirus infections[52,57,58] and showed that UPR reduces flaviviral multiplication,[54] thereby establishing UPR as an anti-flaviviral mechanism. In contrast to flaviviruses, alphaviruses like CHIKV are not susceptible to UPR antiviral mechanisms, as their nsP2 protein inhibits the expression of UPR transcription factors.[73] Accordingly, we did not report any pro-CHIKV function for mosquito EV lipids. UPR activation through infection-induced ER stress triggers phosphorylation of the transcription factor IRE1a, which is localized within the ER membrane.[68] The reactivity of transmembrane proteins depends on the lipid membrane composition,[74] and accordingly, dysregulation of sphingolipid biosynthesis influences UPR activation.[75–77] Supported by our observation that EV lipids elevate SM concentration in the ER, we propose that SMs derived from internalized mosquito EVs alter the ER membrane lipid composition, which in turn hampers IRE1a activation. Lipid transfer within cells occurs through vesicular and non-vesicular pathways[78] and has been specifically documented for SMs,[79] providing a mechanistic rationale for the trafficking of EV-contained SMs to the ER. Upon phosphorylation, IRE1a induces the expression of more than ten ERAD-related genes with different functions, resulting in the transport of identified misfolded proteins to the proteasome for degradation. We reported that mosquito EV lipids inhibit the expression of several ERAD genes, some of which reduce viral protein quantities, providing a rationale for increased viral protein levels when infection was supplemented with mosquito EV lipids. While lipids are involved at each step of the flavivirus cycle,[32,80] lipid reconfigurations have only been associated with promoting flaviviral genome replication.[64,66] Our mechanistic characterization reveals a novel lipid-based mechanism by which flavivirus protein quantity is increased.

Co-inoculation of viruses with EV lipids or SMs in mice resulted in aggravated disease severity. Upon biting, flaviviruses replicate in various skin cell types—prior studies reported infections in fibroblasts,[81,82] keratinocytes,[13,83] dermal DCs,[84,85] and Langerhans cells (LCs).[86] A few hours post biting, virus-permissive myeloid cells are recruited to the bite site, amplifying local infection and triggering systemic spread by migrating to lymph nodes.[12,20,85,87] Our findings revealing that EV-lipid-mediated infection enhancement is consistent across multiple skin cell types, including primary skin fibroblasts and flavivirus-permissive myeloid cells, indicate that salivary EV lipids promote local infection at the bite site. Direct effects of salivary EV components are likely short-lived, as aqueous components delivered in the dermis are absorbed within hours[88] and EVs are usually internalized within hours.[89,90] Our study reports an extensive lipidome reconfiguration as early as 4 h post exposition to EV lipids, which is concomitant with a quantifiable increase in viral proteins at 6 hpi. As prior studies showed that altering the initial skin infection influences transmission and disease severity in mice,[91] we propose a model whereby SMs in mosquito saliva enhance initial skin infection, heightening transmission and disease severity. The pronounced influence of EV-lipid co-inoculation on disease severity further underscores the critical role of initial cutaneous infection in determining overall disease progression.

In conclusion, our discovery of mosquito salivary lipids as pan-flavivirus transmission enhancers changes the paradigm in the intricate interactions between viruses, hosts, and mosquitoes that govern transmission dynamics by introducing lipids as a new category of targetable factors for a new opportunity of much-needed broad-spectrum therapeutics. This is also the first report of a metabolic-based mechanism of transmission enhancement throughout the field of vector-borne diseases. More broadly, while the effects of EV lipids from other organisms start to garner attention,[62] our study provides the evidence that lipids derived from EVs influence viral infection.

Limitations of the study

We used lipids extracted from different batches of EVs, and, although the infection enhancement was reproducible, we observed variability in the intensity of infection increases. The variability may stem from differences in cell culture conditions influencing EV-lipid composition.[62] To inform this potentially confounding effect, we indicated the ID and characteristics of the EV batch that was used in each experiment. Additionally, in our *in vivo* transmission assay, we mimicked bite-initiated transmission by intradermal inoculation, which may not reproduce the complex process of biting. However, methods to completely eliminate salivary lipids *in vivo* are not available.

(E) Experimental design for SMs co-inoculation. *n*, 10 per condition, 9 for no inf.
(F–H) Mean relative weight change ± SEM (F), mean clinical score ± SEM (G), and survival (H) over 12 days post injection.
p indicates differences with CTRL for time × treatment interaction.
See also Figure S4 and Data S1, S2B, and S2C.

RESOURCE AVAILABILITY

Lead contact

Further information and requests for resources and reagents should be directed to and will be fulfilled by the lead contact, Julien Pompon: julien.pompon@ird.fr.

Materials availability

This study did not generate new, unique reagents.

Data and code availability

Global lipidomics data have been deposited in Zenodo: https://doi.org/10.5281/zenodo.10478862. This study did not generate new code. All datasets generated or analyzed during this study are included in the published article. All source data used for the graphs in the manuscript are available as Data S1. Any additional information required to reanalyze the data reported in this paper is available from the lead contact upon request.

ACKNOWLEDGMENTS

We thank Professors Eng Eong Ooi and Mariano Garcia-Blanco for their comments on an earlier version. We extend our gratitude to the members of the Pompon's Laboratory at MIVEGEC, IRD, for their valuable suggestions and support. Special thanks go to Dr. Thierry Durand and Juliette Van-dijk from CNRS, Montpellier, for their assistance. Our appreciation goes to Nathalie Barougier and Drs. Sylvie Cornelie and Idris Mhaidi for their help in mouse management. Additionally, we are grateful to the VectoPole team in Montpellier, particularly Bethsabée Scheid and Carole Ginibre, for providing the mosquito eggs. Lipidomic analyses were performed at MetaToul (Toulouse Metabolomics & Fluxomics Facilities, www.mth-metatoul.com), which is part of the French National Infrastructure for Metabolomics and Fluxomics MetaboHUB-ANR-11-INBS-0010. We are grateful to Nancy Geoffre, Amelie Perez, Océane Delos, and Anaele Durbec for lipid analysis. Support for this research came from fellowships from the Fondation pour la Recherche Médicale to H.M. (SPF202110013925) and to E.F.M. (ARF202309017577), Risques Infectieux et Vecteurs en Occitanie (RIVOC) and Key Initiatives MUSE Risques Infectieux et Vecteurs (KIM RIV) grants to H.M. and J.P., French Agence Nationale pour la Recherche (ANR-20-CE15-0006 to J.P. and ANR-21-CE15-0041 to S.N.), and EU HORIZON-HLTH-2023-DISEASE-03-18 (#101137006) and the French National Facility in Metabolomics & Fluxomics, MetaboHUB (11-INBS-0010) to G.M.

AUTHOR CONTRIBUTIONS

Conceptualization, H.M., J.B.-M., G.M., and J.P.; formal analysis, H.M., L.P., X.G., D.R.S., S.N., E.N.H., J.B.-M., D.M., G.M., and J.P.; funding acquisition, H.M., E.F.M., and J.P.; investigation, H.M., L.P., E.F.M., X.G., V.V., M.T., P.B., J.R., A.H., W.S., J.Z., and G.M.; methodology, H.M., V.V., M.T., P.B., E.N.-'t.H., J.B.-M., G.M., and J.P.; supervision, J.P.; visualization, H.M. and J.P.; writing – original draft, H.M. and J.P.; and writing – review and editing, all authors.

DECLARATION OF INTERESTS

The authors declare no competing interests.

STAR★METHODS

Detailed methods are provided in the online version of this paper and include the following:

- KEY RESOURCES TABLE
- EXPERIMENTAL MODEL AND STUDY PARTICIPANT DETAILS
  - Cells
  - Viruses
  - Mice
  - Mosquitoes
- METHOD DETAILS
  - Collection of saliva- and cell-derived extracellular vesicles (EVs)
  - Flow cytometric analysis of mosquito EV uptake by human cells
  - Extraction of nucleotide-free EV-proteins and EV-lipids
  - Isolation of DENV for lipid extraction
  - Cell infection upon supplementation with intact EVs, EV-proteins, EV-lipids, DENV-lipids, EV-lipid fractions and SM
  - Focus Forming Unit (FFU) assay
  - Relative quantification of viral gRNA
  - Evaluation of cell viability
  - Absolute quantification of DENV and WNV (+) gRNA
  - Attachment and internalization assays
  - Translation assay
  - Replication Assay
  - Relative quantification of total nascent proteins
  - Inhibition of IRE1α-mediated Unfolded Protein Response (UPR)
  - Western blot quantification of IRE1α and phosphorylated-IRE1α
  - Relative quantification of ERAD and IFN-related genes
  - Hrd1, Serl1 L and Herpud1 Silencing
  - Targeted quantitative lipidomics
  - Lipid fractionation
  - Metabolite extraction from cells
  - Untargeted lipidomics
  - Sphingomyelinase (SMase) and Ceramidase (CERase) treatments
  - Sphingomyelin quantification in EVs from mosquito cells and mosquito saliva, and in human cells
  - Cell fractionation
  - Western blot quantification of cytosolic Actin and ER-resident Ribophorin I
  - WNV injection in mice
- QUANTIFICATION AND STATISTICAL ANALYSIS

SUPPLEMENTAL INFORMATION

Supplemental information can be found online at https://doi.org/10.1016/j.cmet.2025.05.015.

Received: September 12, 2024
Revised: March 14, 2025
Accepted: May 29, 2025
Published: June 20, 2025

REFERENCES

1. Pierson, T.C., and Diamond, M.S. (2020). The continued threat of emerging flaviviruses. Nat. Microbiol. *5*, 796–812. https://doi.org/10.1038/s41564-020-0714-0.
2. Bhatt, S., Gething, P.W., Brady, O.J., Messina, J.P., Farlow, A.W., Moyes, C.L., Drake, J.M., Brownstein, J.S., Hoen, A.G., Sankoh, O., et al. (2013). The global distribution and burden of dengue. Nature *496*, 504–507. https://doi.org/10.1038/nature12060.
3. Kraemer, M.U.G., Reiner, R.C., Brady, O.J., Messina, J.P., Gilbert, M., Pigott, D.M., Yi, D., Johnson, K., Earl, L., Marczak, L.B., et al. (2019). Past and future spread of the arbovirus vectors Aedes aegypti and Aedes albopictus. Nat. Microbiol. *4*, 854–863. https://doi.org/10.1038/s41564-019-0376-y.
4. Messina, J.P., Brady, O.J., Golding, N., Kraemer, M.U.G., Wint, G.R.W., Ray, S.E., Pigott, D.M., Shearer, F.M., Johnson, K., Earl, L., et al. (2019). The current and future global distribution and population at risk of dengue. Nat. Microbiol. *4*, 1508–1515. https://doi.org/10.1038/s41564-019-0476-8.
5. Habarugira, G., Suen, W.W., Hobson-Peters, J., Hall, R.A., and Bielefeldt-Ohmann, H. (2020). West Nile Virus: An Update on Pathobiology, Epidemiology, Diagnostics, Control and "One Health" Implications. Pathogens *9*, 589. https://doi.org/10.3390/pathogens9070589.
6. Styer, L.M., Lim, P.-Y., Louie, K.L., Albright, R.G., Kramer, L.D., and Bernard, K.A. (2011). Mosquito Saliva Causes Enhancement of West

Nile Virus Infection in Mice. J. Virol. *85*, 1517–1527. https://doi.org/10.1128/JVI.01112-10.

7. Castanha, P.M.S., Azar, S.R., Yeung, J., Wallace, M., Kettenburg, G., Watkins, S.C., Marques, E.T.A., Vasilakis, N., and Barratt-Boyes, S.M. (2024). Aedes aegypti Mosquito Probing Enhances Dengue Virus Infection of Resident Myeloid Cells in Human Skin. Viruses *16*, 1253. https://doi.org/10.3390/v16081253.
8. Manning, J.E., Morens, D.M., Kamhawi, S., Valenzuela, J.G., and Memoli, M. (2018). Mosquito Saliva: The Hope for a Universal Arbovirus Vaccine? J. Infect. Dis. *218*, 7–15. https://doi.org/10.1093/infdis/jiy179.
9. Marín-López, A., Raduwan, H., Chen, T.-Y., Utrilla-Trigo, S., Wolfhard, D. P., and Fikrig, E. (2023). Mosquito Salivary Proteins and Arbovirus Infection: From Viral Enhancers to Potential Targets for Vaccines. Pathogens *12*, 371. https://doi.org/10.3390/pathogens12030371.
10. Wang, Z.-Y., Nie, K.-X., Niu, J.-C., and Cheng, G. (2024). Research progress toward the influence of mosquito salivary proteins on the transmission of mosquito-borne viruses. Insect Sci. *31*, 663–673. https://doi.org/10.1111/1744-7917.13193.
11. Pingen, M., Schmid, M.A., Harris, E., and McKimmie, C.S. (2017). Mosquito Biting Modulates Skin Response to Virus Infection. Trends Parasitol. *33*, 645–657. https://doi.org/10.1016/j.pt.2017.04.003.
12. Guerrero, D., Cantaert, T., and Missé, D. (2020). Aedes Mosquito Salivary Components and Their Effect on the Immune Response to Arboviruses. Front. Cell. Infect. Microbiol. *10*, 407. https://doi.org/10.3389/fcimb.2020.00407.
13. Surasombatpattana, P., Hamel, R., Patramool, S., Luplertlop, N., Thomas, F., Desprès, P., Briant, L., Yssel, H., and Missé, D. (2011). Dengue virus replication in infected human keratinocytes leads to activation of antiviral innate immune responses. Infect. Genet. Evol. *11*, 1664–1673. https://doi.org/10.1016/j.meegid.2011.06.009.
14. Conway, M.J., Watson, A.M., Colpitts, T.M., Dragovic, S.M., Li, Z., Wang, P., Feitosa, F., Shepherd, D.T., Ryman, K.D., Klimstra, W.B., et al. (2014). Mosquito saliva serine protease enhances dissemination of dengue virus into the mammalian host. J. Virol. *88*, 164–175. https://doi.org/10.1128/JVI.02235-13.
15. Wichit, S., Ferraris, P., Choumet, V., and Missé, D. (2016). The effects of mosquito saliva on dengue virus infectivity in humans. Curr. Opin. Virol. *21*, 139–145. https://doi.org/10.1016/j.coviro.2016.10.001.
16. Schmid, M.A., Glasner, D.R., Shah, S., Michlmayr, D., Kramer, L.D., and Harris, E. (2016). Mosquito Saliva Increases Endothelial Permeability in the Skin, Immune Cell Migration, and Dengue Pathogenesis during Antibody-Dependent Enhancement. PLoS Pathog. *12*, e1005676. https://doi.org/10.1371/journal.ppat.1005676.
17. Cox, J., Mota, J., Sukupolvi-Petty, S., Diamond, M.S., and Rico-Hesse, R. (2012). Mosquito bite delivery of dengue virus enhances immunogenicity and pathogenesis in humanized mice. J. Virol. *86*, 7637–7649. https://doi.org/10.1128/JVI.00534-12.
18. Le Coupanec, A., Babin, D., Fiette, L., Jouvion, G., Ave, P., Misse, D., Bouloy, M., and Choumet, V. (2013). Aedes mosquito saliva modulates Rift Valley fever virus pathogenicity. PLoS Negl. Trop. Dis. *7*, e2237. https://doi.org/10.1371/journal.pntd.0002237.
19. Moser, L.A., Lim, P.-Y., Styer, L.M., Kramer, L.D., and Bernard, K.A. (2016). Parameters of Mosquito-Enhanced West Nile Virus Infection. J. Virol. *90*, 292–299. https://doi.org/10.1128/JVI.02280-15.
20. Pingen, M., Bryden, S.R., Pondeville, E., Schnettler, E., Kohl, A., Merits, A., Fazakerley, J.K., Graham, G.J., and McKimmie, C.S. (2016). Host Inflammatory Response to Mosquito Bites Enhances the Severity of Arbovirus Infection. Immunity *44*, 1455–1469. https://doi.org/10.1016/j.immuni.2016.06.002.
21. Vogt, M.B., Lahon, A., Arya, R.P., Kneubehl, A.R., Spencer Clinton, J.L., Paust, S., and Rico-Hesse, R. (2018). Mosquito saliva alone has profound effects on the human immune system. PLoS Negl. Trop. Dis. *12*, e0006439. https://doi.org/10.1371/journal.pntd.0006439.
22. McCracken, M.K., Gromowski, G.D., Garver, L.S., Goupil, B.A., Walker, K.D., Friberg, H., Currier, J.R., Rutvisuttinunt, W., Hinton, K.L., Christofferson, R.C., et al. (2020). Route of inoculation and mosquito vector exposure modulate dengue virus replication kinetics and immune responses in rhesus macaques. PLoS Negl. Trop. Dis. *14*, e0008191. https://doi.org/10.1371/journal.pntd.0008191.
23. Buezo Montero, S., Gabrieli, P., Montarsi, F., Borean, A., Capelli, S., De Silvestro, G., Forneris, F., Pombi, M., Breda, A., Capelli, G., et al. (2020). IgG Antibody Responses to the Aedes albopictus 34k2 Salivary Protein as Novel Candidate Marker of Human Exposure to the Tiger Mosquito. Front. Cell. Infect. Microbiol. *10*, 377. https://doi.org/10.3389/fcimb.2020.00377.
24. Etienne, V., Gallagher, A., Christofferson, R.C., McCracken, M.K., Cummings, D.A.T., and Long, M.T. (2023). Antibodies to Aedes spp. salivary proteins: a systematic review and pooled analysis. Front. Trop. Dis. *4*. https://doi.org/10.3389/fitd.2023.1145340.
25. Uraki, R., Hastings, A.K., Marin-Lopez, A., Sumida, T., Takahashi, T., Grover, J.R., Iwasaki, A., Hafler, D.A., Montgomery, R.R., and Fikrig, E. (2019). Aedes aegypti AgBR1 antibodies modulate early Zika virus infection of mice. Nat. Microbiol. *4*, 948–955. https://doi.org/10.1038/s41564-019-0385-x.
26. Uraki, R., Hastings, A.K., Brackney, D.E., Armstrong, P.M., and Fikrig, E. (2019). AgBR1 antibodies delay lethal Aedes aegypti-borne West Nile virus infection in mice. npj Vaccines *4*, 23. https://doi.org/10.1038/s41541-019-0120-x.
27. Wang, Y., Marin-Lopez, A., Jiang, J., Ledizet, M., and Fikrig, E. (2020). Vaccination with Aedes aegypti AgBR1 Delays Lethal Mosquito-Borne Zika Virus Infection in Mice. Vaccines *8*, 145. https://doi.org/10.3390/vaccines8020145.
28. Martín-Acebes, M.A., Vázquez-Calvo, Á., and Saiz, J.-C. (2016). Lipids and flaviviruses, present and future perspectives for the control of dengue, Zika, and West Nile viruses. Prog. Lipid Res. *64*, 123–137. https://doi.org/10.1016/j.plipres.2016.09.005.
29. Neufeldt, C.J., Cortese, M., Acosta, E.G., and Bartenschlager, R. (2018). Rewiring cellular networks by members of the Flaviviridae family. Nat. Rev. Microbiol. *16*, 125–142. https://doi.org/10.1038/nrmicro.2017.170.
30. Barrows, N.J., Campos, R.K., Liao, K.-C., Prasanth, K.R., Soto-Acosta, R., Yeh, S.-C., Schott-Lerner, G., Pompon, J., Sessions, O.M., Bradrick, S.S., et al. (2018). Biochemistry and Molecular Biology of Flaviviruses. Chem. Rev. *118*, 4448–4482. https://doi.org/10.1021/acs.chemrev.7b00719.
31. Leier, H.C., Messer, W.B., and Tafesse, F.G. (2018). Lipids and pathogenic flaviviruses: An intimate union. PLoS Pathog. *14*, e1006952. https://doi.org/10.1371/journal.ppat.1006952.
32. Vial, T., Marti, G., Missé, D., and Pompon, J. (2021). Lipid Interactions Between Flaviviruses and Mosquito Vectors. Front. Physiol. *12*, 763195. https://doi.org/10.3389/fphys.2021.763195.
33. Martín-Acebes, M.A., Merino-Ramos, T., Blázquez, A.-B., Casas, J., Escribano-Romero, E., Sobrino, F., and Saiz, J.-C. (2014). The Composition of West Nile Virus Lipid Envelope Unveils a Role of Sphingolipid Metabolism in Flavivirus Biogenesis. J. Virol. *88*, 12041–12054. https://doi.org/10.1128/JVI.02061-14.
34. Diop, F., Vial, T., Ferraris, P., Wichit, S., Bengue, M., Hamel, R., Talignani, L., Liegeois, F., Pompon, J., Yssel, H., et al. (2018). Zika virus infection modulates the metabolomic profile of microglial cells. PLoS One *13*, e0206093. https://doi.org/10.1371/journal.pone.0206093.
35. Leier, H.C., Weinstein, J.B., Kyle, J.E., Lee, J.-Y., Bramer, L.M., Stratton, K.G., Kempthorne, D., Navratil, A.R., Tafesse, E.G., Hornemann, T., et al. (2020). A global lipid map defines a network essential for Zika virus replication. Nat. Commun. *11*, 3652. https://doi.org/10.1038/s41467-020-17433-9.
36. Branche, E., Wang, Y.-T., Viramontes, K.M., Valls Cuevas, J.M., Xie, J., Ana-Sosa-Batiz, F., Shafee, N., Duttke, S.H., McMillan, R.E., Clark, A. E., et al. (2022). SREBP2-dependent lipid gene transcription enhances

the infection of human dendritic cells by Zika virus. Nat. Commun. *13*, 5341. https://doi.org/10.1038/s41467-022-33041-1.

37. Cui, L., Pang, J., Lee, Y.H., Ooi, E.E., Ong, C.N., Leo, Y.S., and Tannenbaum, S.R. (2018). Serum metabolome changes in adult patients with severe dengue in the critical and recovery phases of dengue infection. PLoS Negl. Trop. Dis. *12*, e0006217. https://doi.org/10.1371/journal.pntd.0006217.
38. Gault, C.R., Obeid, L.M., and Hannun, Y.A. (2010). An overview of sphingolipid metabolism: from synthesis to breakdown. Adv. Exp. Med. Biol. *688*, 1–23. https://doi.org/10.1007/978-1-4419-6741-1_1.
39. Jiménez de Oya, N., San-Félix, A., Casasampere, M., Blázquez, A.-B., Mingo-Casas, P., Escribano-Romero, E., Calvo-Pinilla, E., Poderoso, T., Casas, J., Saiz, J.-C., et al. (2023). Pharmacological Elevation of Cellular Dihydrosphingomyelin Provides a Novel Antiviral Strategy against West Nile Virus Infection. Antimicrob. Agents Chemother. *67*, e0168722. https://doi.org/10.1128/aac.01687-22.
40. Martín-Acebes, M.A., Gabandé-Rodríguez, E., García-Cabrero, A.M., Sánchez, M.P., Ledesma, M.D., Sobrino, F., and Saiz, J.-C. (2016). Host sphingomyelin increases West Nile virus infection in vivo. J. Lipid Res. *57*, 422–432. https://doi.org/10.1194/jlr.M064212.
41. Taniguchi, M., Tasaki, T., Ninomiya, H., Ueda, Y., Kuremoto, K.-I., Mitsutake, S., Igarashi, Y., Okazaki, T., and Takegami, T. (2016). Sphingomyelin generated by sphingomyelin synthase 1 is involved in attachment and infection with Japanese encephalitis virus. Sci. Rep. *6*, 37829. https://doi.org/10.1038/srep37829.
42. Yeh, S.-C., Strilets, T., Tan, W.-L., Castillo, D., Medkour, H., Rey-Cadilhac, F., Serrato-Pomar, I.M., Rachenne, F., Chowdhury, A., Chuo, V., et al. (2023). The anti-immune dengue subgenomic flaviviral RNA is present in vesicles in mosquito saliva and is associated with increased infectivity. PLoS Pathog. *19*, e1011224. https://doi.org/10.1371/journal.ppat.1011224.
43. van Niel, G., D'Angelo, G., and Raposo, G. (2018). Shedding light on the cell biology of extracellular vesicles. Nat. Rev. Mol. Cell Biol. *19*, 213–228. https://doi.org/10.1038/nrm.2017.125.
44. Sun, P., Nie, K., Zhu, Y., Liu, Y., Wu, P., Liu, Z., Du, S., Fan, H., Chen, C.-H., Zhang, R., et al. (2020). A mosquito salivary protein promotes flavivirus transmission by activation of autophagy. Nat. Commun. *11*, 260. https://doi.org/10.1038/s41467-019-14115-z.
45. Reddy, T., and Sansom, M.S.P. (2016). Computational virology: From the inside out. Biochim. Biophys. Acta *1858*, 1610–1618. https://doi.org/10.1016/j.bbamem.2016.02.007.
46. Hitakarun, A., Williamson, M.K., Yimpring, N., Sornjai, W., Wikan, N., Arthur, C.J., Pompon, J., Davidson, A.D., and Smith, D.R. (2022). Cell Type Variability in the Incorporation of Lipids in the Dengue Virus Virion. Viruses *14*, 2566. https://doi.org/10.3390/v14112566.
47. Rey-Cadilhac, F., Rachenne, F., Missé, D., and Pompon, J. (2023). Viral Components Trafficking with(in) Extracellular Vesicles. Viruses *15*, 2333. https://doi.org/10.3390/v15122333.
48. Théry, C., Witwer, K.W., Aikawa, E., Alcaraz, M.J., Anderson, J.D., Andriantsitohaina, R., Antoniou, A., Arab, T., Archer, F., Atkin-Smith, G. K., et al. (2018). Minimal information for studies of extracellular vesicles 2018 (MISEV2018): a position statement of the International Society for Extracellular Vesicles and update of the MISEV2014 guidelines. J. Extracell. Vesicles *7*, 1535750. https://doi.org/10.1080/20013078.2018.1535750.
49. Bettis, A.A., L'Azou Jackson, M.L., Yoon, I.-K., Breugelmans, J.G., Goios, A., Gubler, D.J., and Powers, A.M. (2022). The global epidemiology of chikungunya from 1999 to 2020: A systematic literature review to inform the development and introduction of vaccines. PLoS Negl. Trop. Dis. *16*, e0010069. https://doi.org/10.1371/journal.pntd.0010069.
50. Yin, Z., Chen, Y.-L., Schul, W., Wang, Q.-Y., Gu, F., Duraiswamy, J., Kondreddi, R.R., Niyomrattanakit, P., Lakshminarayana, S.B., Goh, A., et al. (2009). An adenosine nucleoside inhibitor of dengue virus. Proc. Natl. Acad. Sci. USA *106*, 20435–20439. https://doi.org/10.1073/pnas.0907010106.
51. Edgil, D., Polacek, C., and Harris, E. (2006). Dengue Virus Utilizes a Novel Strategy for Translation Initiation When Cap-Dependent Translation Is Inhibited. J. Virol. *80*, 2976–2986. https://doi.org/10.1128/JVI.80.6.2976-2986.2006.
52. Peña, J., and Harris, E. (2011). Dengue Virus Modulates the Unfolded Protein Response in a Time-dependent Manner. J. Biol. Chem. *286*, 14226–14236. https://doi.org/10.1074/jbc.M111.222703.
53. Medigeshi, G.R., Lancaster, A.M., Hirsch, A.J., Briese, T., Lipkin, W.I., Defilippis, V., Früh, K., Mason, P.W., Nikolich-Zugich, J., and Nelson, J.A. (2007). West Nile virus infection activates the unfolded protein response, leading to CHOP induction and apoptosis. J. Virol. *81*, 10849–10860. https://doi.org/10.1128/JVI.01151-07.
54. Ambrose, R.L., and Mackenzie, J.M. (2011). West Nile virus differentially modulates the unfolded protein response to facilitate replication and immune evasion. J. Virol. *85*, 2723–2732. https://doi.org/10.1128/JVI.02050-10.
55. Bhattarai, K.R., Riaz, T.A., Kim, H.-R., and Chae, H.-J. (2021). The aftermath of the interplay between the endoplasmic reticulum stress response and redox signaling. Exp. Mol. Med. *53*, 151–167. https://doi.org/10.1038/s12276-021-00560-8.
56. Adams, C.J., Kopp, M.C., Larburu, N., Nowak, P.R., and Ali, M.M.U. (2019). Structure and Molecular Mechanism of ER Stress Signaling by the Unfolded Protein Response Signal Activator IRE1. Front. Mol. Biosci. *6*, 11. https://doi.org/10.3389/fmolb.2019.00011.
57. Reid, D.W., Campos, R.K., Child, J.R., Zheng, T., Chan, K.W.K., Bradrick, S.S., Vasudevan, S.G., Garcia-Blanco, M.A., and Nicchitta, C.V. (2018). Dengue Virus Selectively Annexes Endoplasmic Reticulum-Associated Translation Machinery as a Strategy for Co-opting Host Cell Protein Synthesis. J. Virol. *92*. e01766-17. https://doi.org/10.1128/JVI.01766-17.
58. Umareddy, I., Pluquet, O., Wang, Q.Y., Vasudevan, S.G., Chevet, E., and Gu, F. (2007). Dengue virus serotype infection specifies the activation of the unfolded protein response. Virol. J. *4*, 91. https://doi.org/10.1186/1743-422X-4-91.
59. Hwang, J., and Qi, L. (2018). Quality Control in the Endoplasmic Reticulum: Crosstalk between ERAD and UPR pathways. Trends Biochem. Sci. *43*, 593–605. https://doi.org/10.1016/j.tibs.2018.06.005.
60. Vembar, S.S., and Brodsky, J.L. (2008). One step at a time: endoplasmic reticulum-associated degradation. Nat. Rev. Mol. Cell Biol. *9*, 944–957. https://doi.org/10.1038/nrm2546.
61. Christianson, J.C., Olzmann, J.A., Shaler, T.A., Sowa, M.E., Bennett, E. J., Richter, C.M., Tyler, R.E., Greenblatt, E.J., Harper, J.W., and Kopito, R.R. (2011). Defining human ERAD networks through an integrative mapping strategy. Nat. Cell Biol. *14*, 93–105. https://doi.org/10.1038/ncb2383.
62. Skotland, T., Sagini, K., Sandvig, K., and Llorente, A. (2020). An emerging focus on lipids in extracellular vesicles. Adv. Drug Deliv. Rev. *159*, 308–321. https://doi.org/10.1016/j.addr.2020.03.002.
63. Cajka, T., and Fiehn, O. (2016). Toward Merging Untargeted and Targeted Methods in Mass Spectrometry-Based Metabolomics and Lipidomics. Anal. Chem. *88*, 524–545. https://doi.org/10.1021/acs.analchem.5b04491.
64. Vial, T., Tan, W.-L., Deharo, E., Missé, D., Marti, G., and Pompon, J. (2020). Mosquito metabolomics reveal that dengue virus replication requires phospholipid reconfiguration via the remodeling cycle. Proc. Natl. Acad. Sci. USA *117*, 27627–27636. https://doi.org/10.1073/pnas.2015095117.
65. Liebscher, S., Ambrose, R.L., Aktepe, T.E., Mikulasova, A., Prier, J.E., Gillespie, L.K., Lopez-Denman, A.J., Rupasinghe, T.W.T., Tull, D., McConville, M.J., et al. (2018). Phospholipase A2 activity during the replication cycle of the flavivirus West Nile virus. PLoS Pathog. *14*, e1007029. https://doi.org/10.1371/journal.ppat.1007029.
66. Heaton, N.S., Perera, R., Berger, K.L., Khadka, S., Lacount, D.J., Kuhn, R.J., and Randall, G. (2010). Dengue virus nonstructural protein 3 redistributes fatty acid synthase to sites of viral replication and increases

cellular fatty acid synthesis. Proc. Natl. Acad. Sci. USA *107*, 17345–17350. https://doi.org/10.1073/pnas.1010811107.

67. Pombo, J.P., and Sanyal, S. (2018). Perturbation of Intracellular Cholesterol and Fatty Acid Homeostasis During Flavivirus Infections. Front. Immunol. *9*, 1276. https://doi.org/10.3389/fimmu.2018.01276.
68. Read, A., and Schröder, M. (2021). The Unfolded Protein Response: An Overview. Biology *10*, 384. https://doi.org/10.3390/biology10050384.
69. Diamond, M.S., Sitati, E.M., Friend, L.D., Higgs, S., Shrestha, B., and Engle, M. (2003). A Critical Role for Induced IgM in the Protection against West Nile Virus Infection. J. Exp. Med. *198*, 1853–1862. https://doi.org/10.1084/jem.20031223.
70. Shrestha, B., and Diamond, M.S. (2004). Role of CD8+ T Cells in Control of West Nile Virus Infection. J. Virol. *78*, 8312–8321. https://doi.org/10.1128/JVI.78.15.8312-8321.2004.
71. Shrestha, B., Samuel, M.A., and Diamond, M.S. (2006). CD8+ T Cells Require Perforin To Clear West Nile Virus from Infected Neurons. J. Virol. *80*, 119–129. https://doi.org/10.1128/JVI.80.1.119-129.2006.
72. Graham, J.B., Swarts, J.L., and Lund, J.M. (2017). A Mouse Model of West Nile Virus Infection. Curr. Protoc. Mouse Biol. *7*, 221–235. https://doi.org/10.1002/cpmo.33.
73. Fros, J.J., Major, L.D., Scholte, F.E.M., Gardner, J., van Hemert, M.J., Suhrbier, A., and Pijlman, G.P. (2015). Chikungunya virus non-structural protein 2-mediated host shut-off disables the unfolded protein response. J. Gen. Virol. *96*, 580–589. https://doi.org/10.1099/vir.0.071845-0.
74. Volmer, R., van der Ploeg, K., and Ron, D. (2013). Membrane lipid saturation activates endoplasmic reticulum unfolded protein response transducers through their transmembrane domains. Proc. Natl. Acad. Sci. USA *110*, 4628–4633. https://doi.org/10.1073/pnas.1217611110.
75. Sorli, S.-C., Colié, S., Albinet, V., Dubrac, A., Touriol, C., Guilbaud, N., Bedia, C., Fabriàs, G., Casas, J., Ségui, B., et al. (2013). The nonlysosomal β-glucosidase GBA2 promotes endoplasmic reticulum stress and impairs tumorigenicity of human melanoma cells. FASEB J. *27*, 489–498. https://doi.org/10.1096/fj.12-215152.
76. Spassieva, S.D., Mullen, T.D., Townsend, D.M., and Obeid, L.M. (2009). Disruption of ceramide synthesis by CerS2 down-regulation leads to autophagy and the unfolded protein response. Biochem. J. *424*, 273–283. https://doi.org/10.1042/BJ20090699.
77. Park, W.-J., and Park, J.-W. (2020). The role of sphingolipids in endoplasmic reticulum stress. FEBS Lett. *594*, 3632–3651. https://doi.org/10.1002/1873-3468.13863.
78. Stefan, C.J., Trimble, W.S., Grinstein, S., Drin, G., Reinisch, K., De Camilli, P., Cohen, S., Valm, A.M., Lippincott-Schwartz, J., Levine, T. P., et al. (2017). Membrane dynamics and organelle biogenesis-lipid pipelines and vesicular carriers. BMC Biol. *15*, 102. https://doi.org/10.1186/s12915-017-0432-0.
79. Koivusalo, M., Jansen, M., Somerharju, P., and Ikonen, E. (2007). Endocytic trafficking of sphingomyelin depends on its acyl chain length. Mol. Biol. Cell *18*, 5113–5123. https://doi.org/10.1091/mbc.e07-04-0330.
80. Avota, E., Bodem, J., Chithelen, J., Mandasari, P., Beyersdorf, N., and Schneider-Schaulies, J. (2021). The Manifold Roles of Sphingolipids in Viral Infections. Front. Physiol. *12*, 715527. https://doi.org/10.3389/fphys.2021.715527.
81. Kurane, I., Janus, J., and Ennis, F.A. (1992). Dengue virus infection of human skin fibroblasts in vitro production of IFN-beta, IL-6 and GM-CSF. Arch. Virol. *124*, 21–30. https://doi.org/10.1007/BF01314622.
82. Bustos-Arriaga, J., García-Machorro, J., León-Juárez, M., García-Cordero, J., Santos-Argumedo, L., Flores-Romo, L., Méndez-Cruz, A. R., Juárez-Delgado, F.J., and Cedillo-Barrón, L. (2011). Activation of the innate immune response against DENV in normal non-transformed human fibroblasts. PLoS Negl. Trop. Dis. *5*, e1420. https://doi.org/10.1371/journal.pntd.0001420.
83. López-González, M., Meza-Sánchez, D., García-Cordero, J., Bustos-Arriaga, J., Vélez-Del Valle, C., Marsch-Moreno, M., Castro-Jiménez, T., Flores-Romo, L., Santos-Argumedo, L., Gutiérrez-Castañeda, B., et al. (2018). Human keratinocyte cultures (HaCaT) can be infected by DENV, triggering innate immune responses that include IFNλ and LL37. Immunobiology *223*, 608–617. https://doi.org/10.1016/j.imbio.2018.07.006.
84. Cerny, D., Haniffa, M., Shin, A., Bigliardi, P., Tan, B.K., Lee, B., Poidinger, M., Tan, E.Y., Ginhoux, F., and Fink, K. (2014). Selective susceptibility of human skin antigen presenting cells to productive dengue virus infection. PLoS Pathog. *10*, e1004548. https://doi.org/10.1371/journal.ppat.1004548.
85. Wang, Z., Nie, K., Liang, Y., Niu, J., Yu, X., Zhang, O., Liu, L., Shi, X., Wang, Y., Feng, X., et al. (2024). A mosquito salivary protein-driven influx of myeloid cells facilitates flavivirus transmission. EMBO J. *43*, 1690–1721. https://doi.org/10.1038/s44318-024-00056-x.
86. Wu, S.J., Grouard-Vogel, G., Sun, W., Mascola, J.R., Brachtel, E., Putvatana, R., Louder, M.K., Filgueira, L., Marovich, M.A., Wong, H.K., et al. (2000). Human skin Langerhans cells are targets of dengue virus infection. Nat. Med. *6*, 816–820. https://doi.org/10.1038/77553.
87. Lefteri, D.A., Bryden, S.R., Pingen, M., Terry, S., McCafferty, A., Beswick, E.F., Georgiev, G., Van der Laan, M., Mastrullo, V., Campagnolo, P., et al. (2022). Mosquito saliva enhances virus infection through sialokinin-dependent vascular leakage. Proc. Natl. Acad. Sci. USA *119*, e2114309119. https://doi.org/10.1073/pnas.2114309119.
88. Milewski, M., Manser, K., Nissley, B.P., and Mitra, A. (2015). Analysis of the absorption kinetics of macromolecules following intradermal and subcutaneous administration. Eur. J. Pharm. Biopharm. *89*, 134–144. https://doi.org/10.1016/j.ejpb.2014.11.013.
89. Bonsergent, E., Grisard, E., Buchrieser, J., Schwartz, O., Théry, C., and Lavieu, G. (2021). Quantitative characterization of extracellular vesicle uptake and content delivery within mammalian cells. Nat. Commun. *12*, 1864. https://doi.org/10.1038/s41467-021-22126-y.
90. Groß, R., Reßin, H., von Maltitz, P., Albers, D., Schneider, L., Bley, H., Hoffmann, M., Cortese, M., Gupta, D., Deniz, M., et al. (2024). Phosphatidylserine-exposing extracellular vesicles in body fluids are an innate defence against apoptotic mimicry viral pathogens. Nat. Microbiol. *9*, 905–921. https://doi.org/10.1038/s41564-024-01637-6.
91. Bryden, S.R., Pingen, M., Lefteri, D.A., Miltenburg, J., Delang, L., Jacobs, S., Abdelnabi, R., Neyts, J., Pondeville, E., Major, J., et al. (2020). Pan-viral protection against arboviruses by activating skin macrophages at the inoculation site. Sci. Transl. Med. *12*, eaax2421. https://doi.org/10.1126/scitranslmed.aax2421.
92. Tsugawa, H., Cajka, T., Kind, T., Ma, Y., Higgins, B., Ikeda, K., Kanazawa, M., Vandergheynst, J., Fiehn, O., and Arita, M. (2015). MS-DIAL: data-independent MS/MS deconvolution for comprehensive metabolome analysis. Nat. Methods *12*, 523–526. https://doi.org/10.1038/nmeth.3393.
93. Fraisier-Vannier, O., Chervin, J., Cabanac, G., Puech, V., Fournier, S., Durand, V., Amiel, A., André, O., Benamar, O.A., Dumas, B., et al. (2020). MS-CleanR: A Feature-Filtering Workflow for Untargeted LC-MS Based Metabolomics. Anal. Chem. *92*, 9971–9981. https://doi.org/10.1021/acs.analchem.0c01594.
94. Tsugawa, H., Kind, T., Nakabayashi, R., Yukihira, D., Tanaka, W., Cajka, T., Saito, K., Fiehn, O., and Arita, M. (2016). Hydrogen Rearrangement Rules: Computational MS/MS Fragmentation and Structure Elucidation Using MS-FINDER Software. Anal. Chem. *88*, 7946–7958. https://doi.org/10.1021/acs.analchem.6b00770.
95. Pang, Z., Chong, J., Zhou, G., de Lima Morais, D.A., Chang, L., Barrette, M., Gauthier, C., Jacques, P.-É., Li, S., and Xia, J. (2021). MetaboAnalyst 5.0: narrowing the gap between raw spectra and functional insights. Nucleic Acids Res. *49*, W388–W396. https://doi.org/10.1093/nar/gkab382.
96. Barletta, A.B.F., Silva, M.C.L.N., and Sorgine, M.H.F. (2012). Validation of Aedes aegypti Aag-2 cells as a model for insect immune studies. Parasit. Vectors *5*, 148. https://doi.org/10.1186/1756-3305-5-148.
97. Blanchet, F.P., Stalder, R., Czubala, M., Lehmann, M., Rio, L., Mangeat, B., and Piguet, V. (2013). TLR-4 engagement of dendritic cells confers a

BST-2/tetherin-mediated restriction of HIV-1 infection to CD4+T cells across the virological synapse. Retrovirology *10*, 6. https://doi.org/10.1186/1742-4690-10-6.

98. Maarifi, G., Lagisquet, J., Hertel, Q., Bonaventure, B., Chamontin, C., Fuchs, K., Moncorgé, O., Tauziet, M., Mombled, M., Papin, L., et al. (2021). Alarmin S100A9 restricts retroviral infection by limiting reverse transcription in human dendritic cells. EMBO J. *40*, e106540. https://doi.org/10.15252/embj.2020106540.
99. Lucas, M., Frenkiel, M.-P., Mashimo, T., Guénet, J.-L., Deubel, V., Desprès, P., and Ceccaldi, P.-E. (2004). The Israeli strain IS-98-ST1 of West Nile virus as viral model for West Nile encephalitis in the Old World. Virol. J. *1*, 9. https://doi.org/10.1186/1743-422X-1-9.
100. Kuno, G. (2010). Early history of laboratory breeding of Aedes aegypti (Diptera: Culicidae) focusing on the origins and use of selected strains. J. Med. Entomol. *47*, 957–971. https://doi.org/10.1603/me10152.
101. Vora, A., Zhou, W., Londono-Renteria, B., Woodson, M., Sherman, M.B., Colpitts, T.M., Neelakanta, G., and Sultana, H. (2018). Arthropod EVs mediate dengue virus transmission through interaction with a tetraspanin domain containing glycoprotein Tsp29Fb. Proc. Natl. Acad. Sci. USA *115*, E6604–E6613. https://doi.org/10.1073/pnas.1720125115.
102. van der Vlist, E.J., Nolte-'t Hoen, E.N.M., Stoorvogel, W., Arkesteijn, G.J. A., and Wauben, M.H.M. (2012). Fluorescent labeling of nano-sized vesicles released by cells and subsequent quantitative and qualitative analysis by high-resolution flow cytometry. Nat. Protoc. *7*, 1311–1326. https://doi.org/10.1038/nprot.2012.065.
103. Defourny, K.A.Y., Pei, X., van Kuppeveld, F.J.M., Nolte-T Hoen, E.N.M., and Hoen, E.N.M. (2024). Picornavirus security proteins promote the release of extracellular vesicle enclosed viruses via the modulation of host kinases. PLoS Pathog. *20*, e1012133. https://doi.org/10.1371/journal.ppat.1012133.
104. Hitakarun, A., Khongwichit, S., Wikan, N., Roytrakul, S., Yoksan, S., Rajakam, S., Davidson, A.D., and Smith, D.R. (2020). Evaluation of the antiviral activity of orlistat (tetrahydrolipstatin) against dengue virus, Japanese encephalitis virus, Zika virus and chikungunya virus. Sci. Rep. *10*, 1499. https://doi.org/10.1038/s41598-020-58468-8.
105. Pompon, J., Manuel, M., Ng, G.K., Wong, B., Shan, C., Manokaran, G., Soto-Acosta, R., Bradrick, S.S., Ooi, E.E., Missé, D., et al. (2017). Dengue subgenomic flaviviral RNA disrupts immunity in mosquito salivary glands to increase virus transmission. PLoS Pathog. *13*, e1006535. https://doi.org/10.1371/journal.ppat.1006535.
106. Bligh, E.G., and Dyer, W.J. (1959). A rapid method of total lipid extraction and purification. Can. J. Biochem. Physiol. *37*, 911–917. https://doi.org/10.1139/o59-099.
107. Barrans, A., Collet, X., Barbaras, R., Jaspard, B., Manent, J., Vieu, C., Chap, H., and Perret, B. (1994). Hepatic lipase induces the formation of pre-beta 1 high density lipoprotein (HDL) from triacylglycerol-rich HDL2. A study comparing liver perfusion to in vitro incubation with lipases. J. Biol. Chem. *269*, 11572–11577. https://doi.org/10.1016/S0021-9258(19)78162-9.
108. Lillington, J.M., Trafford, D.J., and Makin, H.L. (1981). A rapid and simple method for the esterification of fatty acids and steroid carboxylic acids prior to gas-liquid chromatography. Clin. Chim. Acta Int. J. Clin. Chem. *111*, 91–98. https://doi.org/10.1016/0009-8981(81)90425-3.
109. Fauland, A., Trötzmüller, M., Eberl, A., Afiuni-Zadeh, S., Köfeler, H., Guo, X., and Lankmayr, E. (2013). An improved SPE method for fractionation and identification of phospholipids. J. Sep. Sci. *36*, 744–751. https://doi.org/10.1002/jssc.201200708.

STAR★METHODS

KEY RESOURCES TABLE

REAGENT or RESOURCE	SOURCE	IDENTIFIER, REFERENCE OR CATALOG NUMBER
Experimental models: Cell lines		
Aedes aegypti Aag2	Provided by D. Missé, MIVEGEC, IRD, Montpellier	N/A
Aedes albopictus C6/36	American Type Culture Collection [ATCC]	CRL-1660
Human hepatocellular carcinoma Huh7	Japanese Health Sciences Foundation, Osaka	JTC-39
Baby Hamster Kidney BHK-21	American Type Culture Collection [ATCC]	CCL-10
African green monkey kidney Vero	American Type Culture Collection [ATCC]	CCL-81
Neonatal Human Dermal Fibroblasts NHDF	Lonza	CC-2509
Monocyte-derived dendritic cells (moDCs)	Produced by S. Nisole Lab, IRIM, CNRS, Montpellier	N/A
Rhesus monkey kidney epithelial LLC-MK2	American Type Culture Collection [ATCC]	CCL-7
Experimental models: Organisms/strains		
Male mice: C57BL/6J	Charles River Laboratories (France)	Cat #C57BL/6J
Irradiation-sterilized mouse diet	A03, SAFE, France	N/A
Animal trimmer	VITIVA MINI, WAHL, BIOSEB, Germany	1584–1693
Imalgène 1000	Boehinger Ingelheim Animal Healt, France	Code: VETO109AA301U
Rompon 2%	Elanco GmbH, Germany	Code: VETO109AA309U
Bacterial and virus strains		
Dengue virus 2 (DENV2); New Guinea C (NGC)	World Reference Center for Emerging Viruses and Arboviruses (WRCREVA) at the University of Texas Medical Branch (UTMB)	N/A
DENV2 strain 16681	D. Smith Lab, Mahidol University, Bangkok, Thailand (Halstead et Simasthien 1970)	N/A
WNV strain IS98-ST1	V. M. Cao-Lormeau and D. Musso, Institut Louis Malardé [ILM], Tahiti Island, French Polynesia	N/A
ZIKV PF-25013-18	V. M. Cao-Lormeau and D. Musso, Institut Louis Malardé [ILM], Tahiti Island, French Polynesia	N/A
CHIKV	P. Duprès, Université de la Réunion, France	N/A
Critical commercial assays		
Primers for qPCR amplification	Eurofins	Table S1
iTaq Universal SYBR Green One-Step Kit	Biorad	1725151
iScript™ gDNA Clear cDNA Synthesis Kit	Biorad	1725035
iTaq Universal Probes One-Step Kit	Biorad	1725141
EvaGreen qPCR Mix	Euromedex	08-25-00001
PrimeScript RT Reagent Kit	Perfect RealTime, Takara Bio Inc.	RR037B
Takyon ROX SYBR MasterMix blue dTTP	Eurogentec	A58667
AllStars Negative Control siRNA FlexiTube	GeneGlobe QIAGEN	GeneGlobe ID: SI03650318
FlexiTube GeneSolution siRNA SEL1L	GeneGlobe QIAGEN	GeneGlobe ID: GS6400
FlexiTube GeneSolution siRNA HERPUD1	GeneGlobe QIAGEN	GeneGlobe ID: GS9709
FlexiTube GeneSolution siRNA SYVN1 (HRD1)	GeneGlobe QIAGEN	GeneGlobe ID: GS84447
DMEM, high glucose, GlutaMAX™ Supplement, pyruvate	Gibco	31966021

(*Continued on next page*)

Continued

REAGENT or RESOURCE	SOURCE	IDENTIFIER, REFERENCE OR CATALOG NUMBER
RPMI 1640 Medium, GlutaMAX™ Supplement	Gibco	61870010
DPBS (1X)	Thermo Fisher Scientific	14190250
FBS	Eurobio	CVFSVF00 01
MEM Non-essential amino acids (NEAA)	Thermo Fisher Scientific	11350912
Penicillin-Streptomycin (P/S)	Thermo Fisher Scientific	11548876
Trypsin - EDTA 0,25%	Thermo Fisher Scientific	25200056
Fibroblast Growth Medium-2 bulletkit (FGM-2)	Lonza	Cat # CC-3132
ReagentPack™ Subculture Reagents	Lonza	Cat # CC-5034
Protease inhibitor cocktail	Roche	11836170001
Phosphatase inhibitor cocktail II	ThermoScientific	J61022
4% paraformaldehyde	Sigma-Aldrich	47608-250ML-F
Methanol	Thermo Fisher Scientific	10010280
Ethanol	Thermo Fisher Scientific	10680993
Chloroform	Sigma-Aldrich	C2432-500ML
Diethylether	J.B-Michel Lab, MetaboHUB-MetaToul, I2MC, INSERM, Toulouse	N/A
Di-isopropylether	J.B-Michel Lab, MetaboHUB-MetaToul, I2MC, INSERM, Toulouse	N/A
DMSO	Sigma-Aldrich	D4540-100ML
Pronase	Sigma-Aldrich	11459643001
Sphingomyelinase (SMase)	Sigma-Aldrich	S8633
RNase A, DNase and protease-free	Thermo Fisher Scientific	EN0531
DNase I recombinant, RNase free	Roche	04716728001
NITD008	Sigma-Aldrich	SML2409-5MG
Tween 20	Sigma-Aldrich	P1379-500ml
MES SDS NuPAGE	Thermo Fisher Scientific	NP0002-02
PageRuler™ Plus Prestained Protein Ladder	Thermo Fisher Scientific	26620
RIPA	Thermo Fisher Scientific	Cat # 89901
Methyl Cellulose	Sigma-Aldrich	M0512-250G
BSA	PAN-Biotech	P06-1391100
40% Acryl/Bisacryl	Euromedex	EU0061-B
Trizma® Base	Sigma-Aldrich	T1503-500G
SDS 20%	Euromedex	EU0660-B
APS	Euromedex	EU0009-B
TEMED	Sigma-Aldrich	T9281-100ML
Trans-Blot Turbo RTA Mini 0.2 μm Nitrocellulose Transfer Kit	Biorad	1704270
SuperSignal™ West Pico PLUS Chemiluminescent Substrate	Thermo Fisher Scientific	34580
Triton X-100	Sigma-Aldrich	X100–100ML
Methanol (HPLC grade)	Fisher Chemicals, Waltham, MA USA	M/4056/15
Acetonitrile (LCMS grade)	Fisher Chemicals, Waltham, MA USA	A/0638/15
Ammonium formate	Hipersolc Chromasolv (VWR chemicals)	84884.180
Formic acid (LCMS grade)	Hipersolc Chromasolv (VWR chemicals)	84865.260
Isopropanol	Fisher Chemicals Waltham, MA USA	P/7500/15
Dichloromethane	32222-2,5L / Fisher	Dichloromethane
Methanol	15631400/ Fisher	2LT Methanol LCMS
Acetic acid	33209-1L/ Merck-Sigma	Acetic acid

(*Continued on next page*)

Continued

REAGENT or RESOURCE	SOURCE	IDENTIFIER, REFERENCE OR CATALOG NUMBER
NL internal standards (stigmasterol; cholesteryl heptadecanoate; glyceryl trinonadecanoate)	Stigmasterol: 1121-k MATREYA; Cholesterol ester C17: BJ492A Interchim; TG57: T4632 Merck	cholesteryl; heptadecanoate; glyceryl trinonadecanoate
PL internal standards (PC 13:0/13:0; Cer d18:1/12:0; PE 12:0/12:0; SM d18:1/12:0; PI 17:0/14:1; PS 12:0/12:0)	PC 13:0/13:0: 850340P / Merck; Cer d18:1/12:0:860512P / Merck; PE 12:0/12:0: 850702P / Merck; SM d18:1/12:0: 860583P / Merck; PI 17:0/14:1: 791641C / Merck; PS 12:0/12:0: 840038P / Merck	N/A
Ethyl acetate	34972-2,5L/Fisher	Ethyl acetate
Ammonium formate	73594-25G-F/ Merck	AMMONIUM ACETATE
deuterium-labeled internal standard [LxA4-d5, LTB4-d4, 5-HETE-d8 (Cayman Chemicals)]	LxA4-d5:10007737/ CAYMAN; LTB4-d4: 320110/CAYMAN; 5-HETE-d8: 334230/ CAYMAN	5(S),6(R)-LIPOXINA4-D5 Article AYR811 1X25ug; LEUKOTRIENE B4-d4; 5(S)-Hydroeicosatetraenoic acid- d8
Internal controls (TG17 or TG19 or TG15)	TG 19 T4632/Sigma	Glyceryl trinonadecanoate
Boron trifluoride methanol	15716-1L /Merck	BORON TRIFLUORIDE METHANOL SOLUTION
Heptane	15624770/ Fisher	2.5LT Heptane LC-MS CHROMASOLV
Acetonitrile	A955212/ Fisher	2.5LT Acétonitrile, Optima
OptiPrep™	STEMCELL Technologies	17109821
PKH26	SIGMA-ALDRICH	MINI26
IRE1 inhibitor III (4μ8C)	Med Chem. Express	Cat. No: HY-19707
enQuireBio™ Recombibant human acid ceramidase protein	Thermo Fisher Scientific	16009460
Lipofectamine RNAiMAX Transfection Reagent	Thermo Fisher Scientific	13778030
Magnesium chloride (MgCl2)	SIGMA-ALDRICH	208337-100G
Calcium chloride (CaCl2)	Thermo Fisher Scientific	L13191.30
Potassium acetate (KOAc)	SIGMA-ALDRICH	P1190-100G
n-Dodecyl β-D-maltoside (DDM)	SIGMA-ALDRICH	D4641-1G
Digitonin	Thermo Fisher Scientific	BN2006
HEPES potassium salt	SIGMA-ALDRICH	H0527-25G
Qubit™ dsDNA High Sensitivity kit	Thermo Fisher Scientific	Q32851
Qubit™ RNA Broad Range (BR) kit	Thermo Fisher Scientific	Q10210
Qubit™ Protein kit	Thermo Fisher Scientific	Q33211
QIAamp Viral RNA Mini Kit	Qiagen	52906
EZNA Total RNA kit I	OMEGA	R6834-03
Sphingomyelin Quantification Colorimetric Assay Kit	Abcam	ab287856
CyQUANT NF Cell Proliferation Assay Kit	Invitrogen	C35007
Protein Synthesis Assay Kit	Abcam	ab239725
Sphingomyelin Assay Kit	Abcam	ab133118
Antibodies		
Mouse Anti-enveloppe (4G2)	Provided by S. Vasudevan from Duke-NUS, Singapore	N/A
Goat Anti-mouse IgG (Alexa Fluor 488)	Life Technologies	A11029
Rabbit anti-DENV2 NS3	Genetex	GTX124252
Mouse anti-Actin	Invitrogen	MA5-11869
Anti-rabbit IgG, HRP-linked	Cell Signaling	7074P2
Anti-mouse IgG, HRP-linked	Cell Signaling	7076P2

(*Continued on next page*)

Continued

REAGENT or RESOURCE	SOURCE	IDENTIFIER, REFERENCE OR CATALOG NUMBER
Rabbit Anti-IRE1α	Cell Signaling	#3294
Rabbit Anti-Phospho-IRE1α	Novus	NB100-2323
Rabbit polyclonal antisera Ribophorin I	Provided by C. Nicchitta, Duke University School of Medicine, USA	N/A
Software and algorithms		
GraphPad Prism		V8.0.2
MS-DIAL	Tsugawa et al.[92]	Version 4.80
MS-CleanR	Fraisier-Vannier et al.[93]	Version 1.0
MS-FINDER	Tsugawa et al.[94]	Version 3.52
MetaboAnalyst	Pang et al.[95]	Version 5.0
Image Lab	Biorad	Version 6.1
Aria Real-Time PCR	Agilent	Version 2.0
Other		
NH2 cartridge HyperSep™ 500mg	Thermo Fisher Scientific	60108-518
OASIS HLB 96-well plate (30 mg/well, Waters)	WAT058951/ UGAP	OASIS HLB 96-well Plate 30 mg Sorbent per Well 30 µm taille particule Reversed-Phase 0 - 14
NexGen™ Mouse 500	Allentown	1304A0078
EVOSTM M5000 microscope	Thermo Fisher Scientific	AMF5000
Applied Biosystems QuantStudio 5	Thermo Fisher Scientific	A34322
AriaMx Real-time PCR System	Agilent	G8830A
Oa-Sys Heating System N-Evap 112 Nitrogen Evaporator	Organomation Associates	N/A
Q Exactive Plus quadrupole (Orbitrap) mass spectrometer	Thermo Fisher Scientific, Hemel Hempstead, U.K.	SN03123L
electrospray probe (HESI II)	Thermo Fisher Scientific, Hemel Hempstead, U.K.	0924783A
U-HPLC Vanquish H system	Thermo Fisher Scientific, Hemel Hempstead, U.K.	8324985
Clarus 600 Perkin Elmer system with FID		N/A
Famewax RESTEK fused silica capillary columns (30 m x 0.32 mm i.d, 0.25 µm film thickness)	12498/ Restek	Colonne capillaire Famewax, L 30m, DI 0.32mm, EF 0.25µm.
Acquity UPLC CSH C18 1.7 µm	Waters SAS, Guyancourt, France	0178321671
Guard column (CSH C18)	Waters SAS, Guyancourt, France	0177321311
ZorBAX SB-C18 column (2.1 mm, 100 mm, 1.8 µm)	RRHD SB-C18, 2,1x100mm, 1,8um, 1200 bars/ Agilent	N/A
GC TRACE 1300 Thermo Electron system with FID	N° de série 717001575/ Thermo Electron	Trace 1300- FID
RTX-5	10223/ Restek	Colonne capillaire Rtx-5, L 30m, DI 0.25mm, EF 0.25µm
Agilent 1290 UPLC system coupled to a G6460 triple quadripole mass spectrometer		N/A
Kinetex HILIC column (Kinetex 2.6 µm HILIC 100 Å, LC Column 50 x 4.6 mm, Ea)	00B-4461-E0/ Phenomenex	N/A
24-well plates	Thermo Fisher Scientific	142475
48-well plates	Thermo Fisher Scientific	150687
Cell culture flask, T-175	SARSTEDT	833912002
Cell culture flask, T-75	SARSTEDT	833911002
0.2 ml non-skirted low profile 96 well PCR plate	Thermo Fisher Scientific	AB-0700
Empty Fastprep® tubes	MP Biomedicals	5076400
Glass beads 1mm	Biospec Products	11079110

EXPERIMENTAL MODEL AND STUDY PARTICIPANT DETAILS

Cells

Aedes aegypti Aag2[96] and baby hamster kidney BHK-21 (CCL-10) cell lines from the American Type Culture Collection (ATCC) were grown in Roswell park memorial institute (RPMI) media (Gibco), supplemented with 10% heat-inactivated fetal bovine serum (FBS) (Gibco) and 1% Penicillin-Streptomycin (P/S) (Gibco) with 5% CO_2 at 28°C for Aag2 and at 37°C for BHK-21. Human hepatocellular carcinoma Huh-7 cell line (clone JTC-39) obtained from the Japanese Health Sciences Foundation, Osaka, Rhesus monkey kidney epithelial LLC-MK2 (CCL-7), and African green monkey kidney Vero (CCL-81) cell line from ATCC were maintained in Dulbecco's modified Eagle medium (DMEM, Gibco), supplemented with 10% FBS, and 1% P/S at 37°C with 5% CO_2. Mosquito cell media was supplemented with 1% non-essential amino acids (NEAA) (Thermo Fisher Scientific). Primary neonatal Human dermal fibroblasts (NHDF) (CC-2509, Lonza) were grown at 37°C with 5% CO_2 in fibroblast growth basal medium (FBM, Lonza) supplemented with fibroblast growth medium-2 bulletkit (FGM-2, Lonza) and 2% FBS (Gibco). All cell lines were yearly tested negative for mycoplasma contamination with specific primers. Buffy coats from healthy donors (n=4) were obtained from the Etablissement Français du Sang (EFS, Montpellier, France). CD14+ monocyte isolation and differentiation to monocyte-derived dendritic cells (moDCs) were performed as previously described.[97,98] MoDCs were maintained in RPMI supplemented with 10% FBS and 1% P/S at 37°C with 5% CO_2.

Viruses

Dengue virus 2 (DENV 2) New Guinea C (NGC) strain and DENV2 16681 strain collected from a dengue fever patient in Thailand were obtained from the World Reference Center for Emerging Viruses and Arboviruses (WRCEVA) at UTMB, TX, USA. West Nile virus (WNV) strain IS98-ST1[99] and chikungunya virus (CHIKV) LR2006_OPY1 strain isolated in la Réunion island were obtained from P. Desprès, University of la Réunion, France. Zika virus (ZIKV) PF-251013-18 strain was obtained via V. M. Cao-Lormeau and D. Musso, Institut Louis Malardé (ILM), Tahiti Island, French Polynesia. All viruses were propagated in C6/36 cells with 2% FBS. DENV productions were titrated using focus forming assay with BHK-21 cells, ZIKV and CHIKV productions were titrated using plaque assay with BHK-21 cells, and WNV was titrated using plaque assay with Vero cells. Viruses were stored at -70°C.

Mice

Five-to-seven-week-old C57BL/6J male mice were purchased from Charles-River (France) and housed in ventilated cages in NexGen Mouse 500 (Allentown; Serial number: 1304A0078) in the biosafety level 3 (BSL-3) animal facility at MIVEGEC-IRD, Montpellier, France. Mice were maintained with 17h:7h light/dark cycle, 53-57% humidity, 20-24°C temperature and provided with irradiation-sterilized mouse diet (A03, SAFE, France) and sterilized water *ad libitum*. Mice were used for experiments one week after reception from Charles-River to let them accommodate to the animal facility. Every effort was made to minimize murine pain and stress. All animal protocols were approved by the APAFiS national ethical committee (permission number: 43466).

Mosquitoes

The BORA *Ae. aegypti* colony collected on Bora-Bora island in 1980[100] was reared in the VectoPole insectary, MIVEGEC. Eggs were hatched in deionized water and larvae were fed grinded fish food (TertraMin, Tetra) at 26°C under 12h:12h light-dark cycle until pupation. Adult mosquitoes were kept in Bioquip cages at 28°C, 70% relative humidity with a 14h:10h light-dark cycle and access to 10% sugar water solution.

METHOD DETAILS

Collection of saliva- and cell-derived extracellular vesicles (EVs)

Bulk saliva collection and EV purification were based on previously described protocols.[44,101] Three pools of saliva samples were collected by allowing **670, 590, and 510** female mosquitoes to feed on a Hemotek feeding system (Discovery Workshops), each containing **3 mL of PBS**. The number of mosquitoes that salivated was estimated by visually counting individuals with enlarged abdomens, indicative of feeding and, consequently, salivation. Saliva pools were combined to total approximately 1,300 **saliva samples**. The saliva solutions were subjected to **ultracentrifugation at 100,000 × g for 155 min**, and the resulting pellet was washed with ice-cold PBS (Gibco). To further eliminate contaminants, the sample underwent a second **ultracentrifugation at 100,000 × g for 155 min** before being resuspended in **100 µL of PBS**.

9 x 10^6 Aag2 cells covering 70-90% of T175 flask surface were reared in complete media. Supernatant was replaced with FBS-free RPMI medium supplemented with 1% P/S and 1% NEAA, and collected after 48h. FBS-free, EV-containing supernatant was centrifugated at 300 x g for 10 min to remove large cell debris, then at 2,000 x g for 10 min to remove small cell debris and finally at 10,000 x g for 30 min to remove large EVs. Supernatant collected from the previous step was ultra-centrifugated at 100,000 x g for 155 min and the pellet was washed with ice-cold PBS (Gibco) before a second ultracentrifugation at 100,000 x g for 155 min to eliminate contaminants. The resulting pellet was resuspended in 800 µl of PBS for EV functional assay, in 20 µl of 0.2 % BSA PBS for the EV uptake assay or in 600-1500 µl 1X Radioimmunoprecipitation Assay (RIPA) buffer (Thermo Scientific) for lipid and protein extractions. Proteins in EV lysates were quantified using Qubit Protein Assay kit (Invitrogen). One µl of EV concentrate solution contained EVs secreted by ≈ 120,000 mosquito cells over 48h and 4.85 µg of protein.

Flow cytometric analysis of mosquito EV uptake by human cells

20 μl of the concentrated mosquito EVs or similarly obtained material from an equal volume of non-conditioned culture medium were stained with 1 μl of PKH26 (Sigma-Aldrich) in 200 μl of diluent C (from the kit). EVs were purified through density gradient by mixing with 60% iodixanol (Opti prep; Axis-Shield) to a final concentration of 45% iodixanol and overlaid with a linear gradient of 40-5% iodixanol in PBS. Density gradients were centrifuged at 190,000 x g for 16 h in SW60 rotor. EV-containing gradient fractions (1.06 g/ml -1.08 g/ml) of 308 μl were collected and EVs were detected by high-resolution flow cytometry using a Cytek Aurora flow cytometer with Enhanced Small Particle module as previously detailed.[102,103] The EV-containing gradient fractions were pooled, diluted with PBS + 0.1% EV-depleted BSA and centrifuged at 190,000 x g for 65 min at 4°C. The EV-containing pellet was resuspended in 150 μl of EV-depleted RPMI and 20 μl of this suspension was added to 10,000 Huh7 cells. As controls, cells were exposed to dye-labelled material from an equal volume of similarly processed non-conditioned medium. At 24h, cells kept at 37°C were detached via trypsinization with 0.05 % trypsin for 5 min at 37°C. Uptake of PKH26-labeled EVs by Huh7 cells was assessed using a Cytek Aurora flow cytometer equipped with three lasers (Cytek Biosciences Inc) with conventional cell acquisition setting. Data analysis was performed using FlowJo v10.07 software (FlowJo LLC, Ashland, OR).

Extraction of nucleotide-free EV-proteins and EV-lipids

Volumes of saliva- or cell-derived EV lysates containing approximately 110 μg of proteins were treated with 2.5 μl of DNAse I recombinant (10 Units/μl) (Roche Diagnostics), 5 μl of 10X DNase buffer, and 10 μl of RNAse A (10 μg/μl) (Thermo Scientific) followed by incubation for 45 min at 37°C. 1 mL of methanol:dichloromethane:nuclease-free water (2:1:1 volume) was then added. The resulting mixture was vortexed for 1 min and centrifuged at 700 x g for 6 min to pellet proteins. The pellet was resuspended in 50 μl of DMSO and corresponded to EV-proteins.

The monophasic liquid phase, containing lipids and other metabolites, was collected, dried under nitrogen and resuspended in 50 μl of DMSO (Sigma-Aldrich). 300 μl of methanol:chloroform (1:1 volume) was added before vortexing for 1h at 4°C. 50 μl of nuclease-free water was added and the resulting solution was vortexed for 1 min and centrifuged at 1,800 x g for 10 min. The protein interphase was added to the previously resuspended protein pellet. The upper organic phase, containing lipids, was dried under nitrogen, resuspended in 50 μl of DMSO and stored at -70°C. DNA, RNA and proteins in the different extracts were quantified using Qubit dsDNA High Sensitivity (HS), Qubit RNA Broad Range (BR) and Qubit Protein Assay kits (Invitrogen), respectively. Several repeats of EV collection and extractions were conducted and details of each collection and extraction are presented in Data S2. 0.1 μl cell EV-lipid extract corresponded to lipids from EVs collected from ≈ 6,000 mosquito cells over 48h.

Isolation of DENV for lipid extraction

Five T175 flasks of C6/36 or LLC-MK2 cells were incubated with DENV2 16681 strain at MOI of 1 for 1h at 28°C for C6/36 or 37°C for LLC-MK2 cells. Mock infections were similarly conducted. On day 3 for LLC-MK2 and day 6 for C6/36, total supernatant was collected. Virions and EVs were precipitated using 10% (w/v) PEG 8,000 (Merck) and 1.5 M NaCl (Merck) at 4°C overnight. After centrifugation at 12,000 x g, the pellet was resuspended in TNE buffer [10 mM Tris-HCl, pH 7.5, 140 mM NaCl, 1 mM EDTA (Bio Basic)] supplemented with 10% (w/v) sucrose (Merck) and layered onto a discontinuous sucrose step gradient, consisting of 30% and 60% sucrose (w/v), creating a 10/30/60 step gradient. Ultra-centrifugation was carried at 82,705 x g for 3.5 h and the fraction immediately above the 60% sucrose cushion was collected, diluted using TNE and pelleted via ultracentrifugation at 82,705 x g for 1.5 h. The resulting pellet was re-suspended in 100 μl of TNE buffer containing 1% BSA. Plaque assay on isolated fractions confirmed the recovery of viruses, as previously published.[104] As control, the same fraction of mock-infected cells was collected. Purifications of DENV and the corresponding controls was performed in Prof. Duncan Smith's Laboratory at Mahidol University, Bangkok, Thailand. Purified virions were shipped in 100% methanol (Merck) on dry ice to IRD, Montpellier, France for lipid extractions as described above.

Cell infection upon supplementation with intact EVs, EV-proteins, EV-lipids, DENV-lipids, EV-lipid fractions and SM

In 24-well plates, 2.5 x 10^5 Huh7, NHDF or moDC cells were incubated with DENV2, WNV, ZIKV or CHIKV at a MOI of 0.1 in 200 μl of FBS-free cell-corresponding media for 1h at 37°C. The inoculum was supplemented with either (i) 0.15 or 1.5 μl of concentrated EVs from saliva, (ii) 0.1 or 1 μl of concentrated EVs from cells, (iii) different quantities of EV-proteins ranging from 0.051–4.85 μg, (iv) 0.1 or 1 μl of salivary EV-lipid extracts, (v) 0.01, 0.1 or 1 μl of cell EV-lipid extracts, (vi) 0.1 μl or 1 μl of DENV-lipid extracts, (vii) 0.1 μl of EV-lipid fractions or (viii) 0.01, 0.1 or 1 μl of a sphingomyelin (SM) solution obtained by resuspending 25 μg of commercial SM pig brain powder in 5 ml of nuclease-free water. To homogenize volumes of DMSO used as vehicle for EV-protein extracts, EV-lipid extracts, DENV-lipids and EV-lipid fractions, the different supplemented volumes were complemented to 1 μl with DMSO. Controls for intact cell-derived EVs were supplemented with 1 μl of PBS; for saliva-derived EVs with 1.5 μl; for SM solutions were supplemented with 1 μl of nuclease-free water; controls for EV-lipid extracts were supplemented with 1 μl of DMSO; controls for DENV-lipids were supplemented with the same volume of lipid extracts from the same fraction of mock-infected cells; controls for EV-lipid fractions were supplemented with 0.1 μl of the corresponding blank extracts resuspended in 1 μl DMSO; and controls for EV-protein extracts were supplemented with 1 μl of DMSO. After incubation, 200 μl of 2% FBS cell-corresponding media was added. At 72h post-infection with DENV, WNV and ZIKV, and 48 h for CHIKV, cells were lysed in 350 μl of TRK lysis buffer (EZNA RNA Kit I, Omega) and supernatant was collected.

Focus Forming Unit (FFU) assay

100,000 BHK-21 cells per well of 24-well plates were incubated with 150 μl of 10-fold serial dilutions of inoculum for 1h at 37°C with 5% CO_2. After removing the inoculum, 500 μl of sterile 2% Carboxymethyl Cellulose (CMC) in RPMI supplemented with 2% FBS and 1% P/S was added. Three days later, cells were fixed with 4% paraformaldehyde (Sigma-Aldrich) for 30 min, permeabilized with 0.3% Triton X-100 (Sigma-Aldrich) PBS for 30 min, stained with pan-flavivirus 4G2 antibody (kindly provided by S. Vasudevan from Duke-NUS, Singapore) at 1:400 in 1% BSA (PAN-Biotech) for 1h at 37°C, and stained with secondary anti-mouse Alexa Fluor 488-conjugated antibody (Invitrogen) at 1:500 in 1% BSA for 1h at 37°C in the dark. Foci were counted using EVOS M5000 imaging system (ThermoFisher) and averaged over three replicates to calculate FFU/ml.

Relative quantification of viral gRNA

Total RNA from cells was extracted using EZNA Total RNA kit I (Omega). Relative quantification of the positive strand of viral gRNA for DENV, ZIKV, WNV and CHIKV was obtained by two-step RT-qPCR. RNA extracts were treated with DNAse and reversed transcribed using gDNA Clear cDNA Synthesis kit (Bio-Rad). qPCR was conducted in 10 μl final volume with 2 μl of cDNA, 2 μl of 5X HOT Pol EvaGreen qPCR mix plus (Euromedex), 300 nM of forward and reverse primers (Table S1) in AriaMx Real-time PCR System (Agilent) with the following thermal conditions: 95°C for 15 min, 45 cycles at 95°C for 15s, 60°C for 20s and 72°C for 20s, followed by a melting curve analysis. *GAPDH* mRNA levels were quantified by qPCR in the same conditions for normalization. Gene expression fold change was calculated by the ΔΔCq method.

Evaluation of cell viability

At 72h post treatment, cell viability was estimated by calculating the inverse differences in GAPDH *Ct* relative to the control conditions and the number of viable cells was evaluated using CyQUANT NF Cell Proliferation Assay Kit (Invitrogen).

Absolute quantification of DENV and WNV (+) gRNA

Total RNA was extracted from cell lysates using EZNA RNA extraction kit I or from blood samples using QIAamp Viral RNA Mini Kit (Qiagen). Absolute quantification of positive strand gRNA was performed through one-step RT-qPCR. Total reaction volume was 10 μl and contained 5 μl of iTaq Universal SYBR green one-step kit (Bio-Rad), 300 nM of forward and reverse primers (Table S1) and 2 μl of RNA extract. The reaction was performed in AriaMx Real-time PCR System with the following thermal profile: 50°C for 10 min, 95°C for 1 min and 40 cycles of 95°C for 10 sec and 60°C for 15 sec, followed by a melting curve analysis. An absolute standard curve for DENV and WNV gRNA was generated by amplifying the qPCR target using primers detailed in Table S1 as performed previously.[42,105]

Attachment and internalization assays

For attachment assay, 2.5×10^5 Huh7 cells prechilled at 4 °C for 15 min were incubated with DENV2 NGC at a MOI of 0.1 in 200 μl of serum-free DMEM supplemented with 0.1 μl of EV-lipid extract complemented with DMSO to 1 μl or 1 μl of DMSO (control) for 30 min at 4 °C. Inoculum was removed and cells were washed thrice with prechilled 2 % FBS DMEM. Attached viruses were quantified as gRNA copies in cell lysates extracted using EZNA RNA extraction kit I. For internalization assay, Huh7 infection was repeated and non-internalized virus particles were removed by adding 2 mg/ml of pronase (Sigma-Aldrich) in 200 μl of serum-free medium for 5 min on ice. After two washes, internalized viruses were quantified as gRNA copies in cell lysate extracted with EZNA RNA extraction kit I.

Translation assay

DENV infection of Huh7 or NHDF cells supplemented with 0.1 μl of EV-lipids was conducted as described above. At 3, 4, 5, and 6h for Huh7 and at 6h for NHDF post-infection, cells were washed twice with PBS, scrapped in 70 μl of RIPA with 1X protease inhibitors (Sigma-Aldrich) and supernatant was collected after centrifugation at 12,000 g for 1 min. Normalized protein quantities were separated under denaturing conditions in 10% polyacrylamide gel and transferred onto 0.2 μm nitrocellulose membrane using TransBlot system (BioRad). Staining was conducted with 1:2,000 anti-DENV2 NS3 (GTX124252, Genetex) and 1:400 anti-Actin (MA5-11869, Invitrogen), and 1:2,000 of goat anti-rabbit (7074P2, Cell Signaling) and goat anti-mouse (7076P2, Cell Signaling) as secondary antibodies, respectively, in PBS-tween 0.1% with 1% BSA.

Translation assay was repeated in Huh7 cells by adding 20 μM of NITD008 (Sigma-Aldrich) in cell media for 2h before infection and during the course of infection. Samples were collected 6 post-infection.

Replication Assay

DENV infection of Huh7 cells supplemented with 0.1 μl of EV-lipids was conducted as described above. At 1, 3, 6, 9, 12, 15, 18, 21 and 24h post-infection, Huh-7 cells were washed with PBS and lysed in 350 μl of TRK lysis buffer. Total RNA was extracted using EZNA Total RNA extraction kit I and used for relative quantification of the negative strand of DENV gRNA [(-)gRNA] using two-step RT-qPCR with TaqMan probe. RNA extracts were treated with DNAse and reversed transcribed using gDNA Clear cDNA Synthesis kit (Bio-Rad). qPCR was conducted in total reaction volume of 10 μl containing 2 μl of cDNA, 5 μl of 2X iTaq Universal probe kit (Bio-Rad), 300 nM of forward and reverse primers and 200 nM of probe (Table S1) in AriaMx machine with the following thermal conditions: 95°C for 2 min followed by 45 cycles of 95°C for 10 sec and 60°C for 30 sec. *GAPDH* mRNA was quantified as above for normalization.

Replication assay was repeated by adding 20 μM of NITD008 (Sigma-Aldrich) in cell media for 2h before infection and during the course of infection. Samples were collected 6 post-infection.

Relative quantification of total nascent proteins

DENV infection of Huh7 supplemented with 0.1 μl of EV-lipids or of DMSO was conducted described above. At 6h post-treatment (hpt), nascent proteins were quantified using Protein Synthesis Assay Kit (Abcam). Briefly, the media was replaced with 1X Protein Label solution and cells were incubated for 1.25 h at 37 °C. Negative controls were not exposed to the Protein Label solution and treatment. Positive controls were incubated with 1X Protein Label solution without treatment. After washing with 100 μl of PBS, 100 μl of Fixative Solution was added and incubated for 15 min at room temperature (RT) in the dark. After washing with 200 μl of 1X Wash Buffer (WB), cells were treated with 100 μl of 1X Permeabilization Buffer (PB) for 10 min at RT, then with 100 μl of 1X reaction cocktail (97 μl PBS, 1 μl of 100X Copper Reagent, 1 μl of 100X Fluorescent Azide and 1 μl 20X Reducing Agent) for 40 min at RT in the dark. Finally, after 2 washes in 200 μl of WB, 100 μl of PBS was added to each well before measuring fluorescence intensity at excitation/emission of 430/535 nm using a Spark multimode microplate reader (TECAN). Relative quantities were obtained by subtracting values from negative controls and normalizing to cells treated with DMSO values.

Inhibition of IRE1α-mediated Unfolded Protein Response (UPR)

2 x 10^5 Huh7 cells were treated with 30 or 60 μM of 4μ8C (MedChemExpress) for 2h before infection with DENV at a MOI of 0.1. Controls were treated with DMSO before infection. At 8 hpt, i.e. 6 hpi, cells were washed with PBS, scrapped in 70 μl of RIPA containing 1X protease and 1X phosphatase inhibitors.

Western blot quantification of IRE1α and phosphorylated-IRE1α

DENV infection of Huh7 cells supplemented with 0.1 μl of EV-lipids was conducted as described above. At 6 hpt, cells were washed with PBS, scrapped in 70 μl of RIPA containing 1X protease and 1X phosphatase inhibitors. WB was conducted as described above for translation assay and staining was performed with 1:500 anti-IRE1α (#3294, Cell Signaling), 1:700 anti-pIRE1 α (NB100-2323, novus) and 1:400 anti-Actin (MA5-11869, Invitrogen), and 1:2,000 of goat anti-rabbit and goat anti-mouse as secondary antibodies.

Relative quantification of ERAD and IFN-related genes

DENV infection of Huh7 cells supplemented with 0.1 μl of EV-lipids was conducted as described above. Total RNA from cells was extracted using EZNA Total RNA kit I. Expression for *Serl1 L, Derlin1, Edem1, Herpud1, Hrd1* and *GAPDH* was quantified through one-step RT-qPCR using iTaq Universal SYBR green one-step kit (Bio-Rad) with the corresponding primers (Table S1) and the conditions described above for WNV (+)gRNA. Relative quantification was performed using the 2-ΔΔCt method by normalization to *GAPDH* Ct values.

Expression for IFN-related genes was conducted by reverse transcription using the PrimeScript RT Reagent Kit (Perfect RealTime, Takara Bio Inc.). qPCR reaction was performed in duplicate using Takyon ROX SYBR MasterMix blue dTTP (Eurogentec) on an Applied Biosystems QuantStudio 5 (Thermo Fisher Scientific) in 384-well plates. Transcripts were quantified using the following program: 3 min at 95°C followed by 35 cycles of 15 s at 95°C, 20 s at 60°C, and 20 s at 72°C. Values for each transcript were normalized to the geometric mean of Ct values of 4 different housekeeping genes (RPL13A, ACTB, B2M, and GAPDH), using the 2-ΔΔCt method. Primers used for quantification of transcripts by qPCR are listed in Table S1.

Hrd1, Serl1 L and Herpud1 Silencing

2 x 10^5 Huh7 cells were transfected overnight with 12 pmol of multiplex siRNAs (Qiagen) using Lipofectamine RNAiMax (ThermoFisherScientific). siRNA GS84447 against *Hrd1*; siRNA GS6400 against *Serl1L*; siRNA GS9709 against *Herpud1* (Table S1) were used. As a control, Allstars multiplex siRNAs (Qiagen) were similarly transfected. 48 h later, cells were infected with DENV as described above. At 6hpi, cells were collected in TRK or RIPA lysis buffers for RNA or protein extractions, respectively.

Targeted quantitative lipidomics

Aag2 EVs isolated as detailed above were lysed in RIPA buffer. Quantification was performed for major phospholipids (PL) [including phosphatidylserine (PS), phosphatidylethanolamine (PE), phosphatidylcholine (PC) and phosphatidylinositol (PI)], major sphingolipids [including ceramide (Cer) and sphingomyelin (SM)], neutrals lipids (NL) [including cholesterol (Chol), cholesterol ester (Chol E) and triacylglycerol (TAG)] and total fatty acids (FA) [including saturated fatty acids (SAFA), monounsaturated fatty acid (MUFA) and polyunsaturated fatty acid (PUFA)]. 200 μg protein equivalent of EV lysates were extracted and analyzed with different methods for each lipid class.

For PL and NL, EV lysates were extracted according to Bligh and Dyer[106] in dichloromethane:water:methanol (2.5:2:2.5, v/v/v) with 2% acetic acid in the presence 100 μl of NL internal standards (stigmasterol; cholesteryl heptadecanoate; glyceryl trinonadecanoate) and 40 μl of PL internal standards (PC 13:0/13:0; Cer d18:1/12:0; PE 12:0/12:0; SM d18:1/12:0; PI 17:0/14:1; PS 12:0/12:0). Samples were centrifugated at 500 x g for 6 min, evaporated to dryness and resuspended in 20 μl of ethyl acetate for NL analysis and 50 μl of methanol for PL analysis. For NL analysis, 1 μl of extract was analyzed by gas-chromatography flame-ionization-detector (GC-FID) on a GC TRACE 1300 Thermo Electron system using an Zebron ZB-5MS Phenomenex columns (5% polysilarylene, 95% polydimethylsiloxane, 5m X 0.25 mm i.d., 0.25 μm film thickness).[107] Oven temperature was programmed from 190°C to 350°C at a rate of 5°C/min

and the carrier gas was hydrogen (5 ml/min). The injector and the detector were at 315°C and 345°C, respectively. For PL analysis, 2 μl of extract was analyzed using an Agilent 1290 UPLC system coupled to a G6460 triple quadripole mass spectrometer (Agilent Technologies). A Kinetex HILIC column (Phenomenex, 50 x 4.6 mm, 2.6 μm) was used for LC separations. The column temperature was controlled at 40°C. The mobile phase A was acetonitrile and the mobile phase B was 10 mM ammonium formate in water at pH 3.2. The gradient was as follow: from 10% to 30% B in 10 min; 10–12 min, 100% B; and then back to 10% B at 13 min for 2 min prior to the next injection. The flow rate of mobile phase was 0.3 ml/min. Electrospray ionization was performed in positive mode for Cer, PE, PC and SM analysis and in negative mode for PI and PS analysis. Needle voltage was set respectively at 4 kV and -3.5 kV. Approximate quantification was obtained for each species through comparison to the internal standards of the concerned lipid family.

For total FA, approximate quantification concerns conventional FA: c10:0, c12:0, c14:0, c15:0, c16:0, c17:0, c18:0, c20:0, c22:0, c23:0, c24:0, c14:1w5, c15:1, c16:1w7, c18:1w9, c18:1w7, c20:1w9, c22:1w9, c24:1w9, c18:2w6, c18:3w6, c18:3w3, c20:2w6, c20:3w3, c20:3w6, c20:4w6, c20:5w3, c22:2w6, c22:6w3, c22:4w6. EV lysates were extracted as described above according to Bligh and Dyer method in the presence of internal controls (TAG19). Samples were centrifugated at 500 x g for 6 min, hydrolyzed in KOH (0.5 M in methanol) at 55°C for 30 min, and transmethylated in 14% boron trifluoride methanol (Sigma) and heptane (Sigma) at 80°C for 1h. Water and heptane were added. Samples were centrifugated at 500 x g for 1 min, dried and resuspended in 20 μl of ethyl acetate. 1 μl of extract was analyzed by GC-FID[108] on a Clarus 600 Perkin Elmer system using a Famewax RESTEK fused silica capillary columns (30 m x 0.32 mm i.d, 0.25 μm film thickness). Oven temperature was programmed from 100°C to 250°C at a rate of 6°C/min and the carrier gas was hydrogen (1.5 ml/min). The injector and the detector were at 220°C and 230°C respectively.

Peak detection, integration and quantitative analysis were done using Mass Hunter quantitative analysis software (Agilent Technologies) based on quantity of internal standards.

Lipid fractionation

NH2 cartridge HyperSep 500 mg (Thermo Fisher Scientific) were conditioned by adding 2 ml of chloroform:methanol (23:1 volume) followed by 2 ml of diethyl ether. 2 x 100 μl of EV-lipid extracts resuspended in diethyl ether were loaded into the cartridge sequentially. Solvents with increasing polarity were used to elute different classes of lipids from the cartridge, as previously described.[109] Briefly, the 6 solvents used were: 2 ml of diethyl ether (F1), 1.6 ml of chloroform:methanol (23:1 volume) (F2), 1.8 ml of diisopropyl ether:acetic acid (98:4 volume) (F3), 2 ml of acetone:methanol (9:1.2 volume) (F4), 2 ml of chloroform:methanol (2:1 volume) (F5) and 2 ml of methanol with 0.2 M of ammonium acetate (F6). Controls were generated by eluting an empty cartridge with the same solvents. Each fraction was dried before resuspension in 50 μl of DMSO.

Metabolite extraction from cells

DENV infection of Huh7 cells supplemented with 0.1 μl of EV-lipids was conducted as described above. Four hours post-treatment, Huh-7 cells were washed with 0.9% NaCl (Sigma) and 4 wells per condition were collected in 500 μl of ice-cold methanol (LC-MS grade, Thermo Fisher Scientific) and water in 80:20 ratio (v/v) by scraping, and sonicated in an ultrasonic bath (J.R. selecta) for 15 min at 4 °C. Samples were centrifuged at 10,000 x g for 1 min at 4 °C, and 400 μl of supernatant was collected. Pellets were extracted a second time by adding 500 μl of methanol:water (80:20 volume) solution, sonicated and centrifuged before collecting another 400 μl of supernatant. Combined supernatants were dried, weighted and stored at -70 °C.

Untargeted lipidomics

Lipid fractions and metabolites extracted from Huh7 cells were analyzed. A Q Exactive Plus quadrupole (Orbitrap) mass spectrometer, equipped with a heated electrospray probe (HESI II) and coupled to a U-HPLC Vanquish H system (Thermo Fisher Scientific, Hemel Hempstead, U.K.) was used for Ultra-High-Performance Liquid Chromatography–High-Resolution Mass Spectrometry (UHPLC-HRMS) profiling. Dry extracts were normalized to 2 mg of dry mass/ml in an 80:20 (v:v) methanol:water solution. Separation was conducted using an Acquity UPLC CSH C18 (100 mm, 2.1 mm, 1.7 μm) equipped with a guard column (Waters SAS). The mobile phase A (MPA) consisted in a mixture of acetonitrile/water (60:40; v/v) with 10 mM ammonium formate and 0.1% formic acid. The mobile phase B (MPB) consisted in an acetonitrile/isopropanol (90:10; v/v) with 10 mM ammonium formate and 0.1% formic acid. The solvent gradient was set as follow: 40% to 43% MPB (0 - 2 min), 50% MPB (2.1 min) to 54% MPB (2.1 – 11.9 min), 70% MPB (11.9 - 12 min), 70% to 99% MPB (12 – 17.9 min), 99% MPB (17.9 – 19.9 min). The flow rate was set to 0.3 mL/min, the autosampler temperature was 5 °C, the column temperature was 55 °C, and injection volume was 1 μl. Mass detection was performed in positive ionization (PI) mode (MS1 resolution power = 35 000 [full width at half-maximum (fwhm) at 400 m/z]; MS2 resolution power = 17 500; MS1 automatic gain control (AGC) target for full scan = 1 $x10^6$; $1x10^5$ for MS2). Ionization spray was set to a 3.5 kV voltage, and the capillary temperature was 256 °C. The mass scanning range was m/z 100–1500. Data-dependent acquisition of MS/MS spectra for the six most intense ions followed each full scan. Stepped normalized collision energy of 20, 40, and 60 eV was used for data acquisition in data dependent analysis mode.

MS-DIAL v. 4.80[92] was used for UHPLC-HRMS raw data analysis. Mass feature extraction ranged between 100 and 1500 Da and 0.5 to 18.5 min. MS1 and MS2 tolerance in centroid mode were set to 0.01 and 0.05 Da, respectively. Optimized detection threshold was set to 10^6 and 10 for MS1 and MS2, respectively. Peaks were aligned to a quality control (QC, aliquot of all sample extracts) reference file, with a retention time tolerance of 0.15 min and a mass tolerance of 0.015 Da. The LipidBlast internal MS-DIAL database was used for putative annotation. MS-CleanR workflow version 1.0[93] was employed for cleaning MS-DIAL data. A minimum blank ratio of 0.8, a maximum relative standard deviation (RSD) of 40, and a relative mass defect (RMD) ranging from 50 to 3000 were

set for all filters selected. For feature relationships detection, the maximum mass difference was set to 0.005 Da, and the maximum RT difference to 0.025 min. The Pearson correlation links were considered with correlation $\geq$ 0.8 and statistically significant with α = 0.05. The most intense and the most connected peaks were kept in each cluster. Feature not annotated within MS-DIAL were elucidated with MS-FINDER version 3.52.[94] The MS1 and MS2 tolerances were respectively set to 5 and 10 ppm. Formula finder was only processed C, H, O, N, P, and S atoms. The databases (DBs) were constituted from MS-FINDER internal DBs with LipidMaps and HMDB. Data were normalized by autoscaling before selecting regulated metabolites with more than two-fold intensity change and p-value < 0.1, as indicated by an unpaired t test with false-discovery rate (FDR) adjustment using MetaboAnalyst (v. 5.0).[95]

For lipid fractions, relative proportion of each class in the different fractions was represented. Total of relative proportions within each lipid class equals 100%. For Huh7 cells exposed to EV-lipids, DENV or both, the significantly regulated lipids were presented in a heatmap.

Sphingomyelinase (SMase) and Ceramidase (CERase) treatments

1µl of commercial SM solution (5 µg/ml), 0.1 µl of mosquito EV-lipid extract or 0.1 µl of EV-lipid fraction 6 was treated with 1 U of SMase (Sigma) for 1h at 37°C, then heated for 30 min at 65°C to inactivate SMase. 0.1 µl of mosquito EV-lipids was treated with 0.25 µg of CERase (Thermo Fisher Scientific) as for SMase treatment. Controls received same quantity of heat-treated SMase or CERase. The resulting solutions were used for supplementation during infection as described above.

Sphingomyelin quantification in EVs from mosquito cells and mosquito saliva, and in human cells

Mosquito cell EVs were isolated as described above by ultracentrifugation and resuspended in 50 µl of SM assay buffer. Two pools of saliva were collected by allowing 400 and 825 female mosquitoes to feed on a Hemotek feeding system, as detailed above. The saliva solutions were ultracentrifugated at 100,000 x g for 155 min and the pellets were resuspended in 30 and 60 µl of SM assay buffer, respectively. 10 µl of cell EV solution (produced by 9 x 10^5 and 9.88 x 10^5 cells) or of salivary EV solution (corresponding to saliva samples from 93 and 137.5 mosquitoes) from each saliva pools were quantified with the SM assay. DENV infection of Huh7 or NHDF cells supplemented with 0.1 µl of EV-lipids was conducted as described above. Two wells per condition were collected in 400 µl of methanol: water (80:20 volume) by scraping. Metabolites were extracted as described above, then dried under nitrogen flux before to be resuspended in 50 µl SM assay buffer.

Absolute SM quantification was obtained with Sphingomyelin Quantification Colorimetric Assay Kit (Abcam) using an absolute standard equation generated from the reagents. To exceed the kit detection threshold, 1 nmol of standard SM was added to each sample. After adjusting sample volume to 50 µl with SM assay buffer, 34 µl SM Assay Buffer, 2 µl Sphingomyelinase, 10 µl ALP Enzyme, 2 µl SM Enzyme Mix, and 2 µl OxiRed Probe were added. Plates were incubated at 37°C for 2h before measuring absorbance at 570 nm using a Spark multimode microplate reader (TECAN). SM quantities in the samples were calculated by subtracting values for 1 nmol of SM standard.

Cell fractionation

At 4 hpt, cells were subjected to sequential detergent extraction of the cytosol and endoplasmic reticulum (ER).[57] Briefly, the cell medium was removed, and the cells were washed with PBS. The cytosolic fraction was extracted by adding 0.15 ml of buffer containing 0.03% digitonin, 110 mM potassium acetate (KOAc), 25 mM K-HEPES (pH 7.2), 15 mM MgCl2, and 4 mM CaCl2. The cells were incubated on ice for 5 min. The buffer was then collected, and the cells were washed with the same buffer containing 0.0015% digitonin, using the same volume. The first lysis and the wash were combined, representing the cytosolic fraction of the cells. The ER fraction was then collected by lysing the digitonin-extracted cells with 0.15 ml of an ER lysis buffer containing 2% Dodecyl-β-D-maltoside (DDM), 200 mM KOAc, 25 mM K-HEPES (pH 7.2), 15 mM MgCl2, and 4 mM CaCl2. For each sample, an equivalent volume of cold methanol:water:dichloromethane (2:1:1) was added, mixed thoroughly, sonicated for 15 min at 4 °C. The sample was centrifuged at 2500 × g for 6 min at 4 °C, and the supernatant was collected, dried, and collected in 50 µl of SM assay buffer to quantify the SMs. The protein pellets were collected in 100 µl RIPA buffer, and used in immunoblot to verify the fractionation protocol, i.e. the efficient separation and recovery of cytosolic (Actin) and ER-resident (Ribophorin I) proteins.

Western blot quantification of cytosolic Actin and ER-resident Ribophorin I

On each fraction, WB was conducted as described above for translation assay. The staining was performed with 1:200 rabbit polyclonal antisera recognizing Ribophorin I (kindly provided by Prof. Christopher Nicchitta, Duke University School of Medicine, USA) and 1:400 anti-Actin (MA5-11869, Invitrogen), and 1:2000 of goat anti-rabbit and goat anti-mouse as secondary antibodies.

WNV injection in mice

Mice were shaved with the animal trimmer (VITIVA MINI, BIOSEB) on the lower back one day prior injection to limit any effect of shaving-induced inflammation. Mice anesthetized by injection of 0.2 ml/mouse of a solution containing 10 mg/ml of ketamine (Imalgène 1000, Boehringer Ingelheim Animal Health) and 1 mg/ml of xylazine (Rompon 2%, Elanco GmbH) were intradermally (ID) inoculated with 10^3 PFU of WNV mixed with 0.1 or 1 µl of mosquito EV-lipid extract complemented to 1 µl with DMSO, or with 1 or 5 µl SM (1 µg/ml) plus 1 µl of DMSO. Total volume injected was complemented to 10 µl with PBS. Control mice were injected with 1 µl of DMSO with or without WNV inoculum in a total volume of 10 µl complemented with PBS. Mice were weighed before injection and daily thereafter to calculate the percent of weight loss. Daily clinical examinations were conducted and a clinical score (CS) ranging from 0 to 5

was assigned to each mouse following criteria from a previous study,[72] where CS of 0 was assigned to healthy mice; CS of 1 for mice with ruffled fur, lethargy, hunched posture, no paresis, normal gait; CS of 2 for mice with altered gait, limited movement in 1 hind limb; CS of 3 for lack of movement, paralysis in 1 or both hind limbs, and CS of 4 for moribund mice. A CS of 5 indicated mortality. At days 2, 4, 6, 8, and 10, blood samples were collected via mandibular puncture and sample volumes were estimated by pipetting. Mice were euthanized if they displayed neurological symptoms, severe distress, or weight loss exceeding 20%. Mice were euthanized under anaesthesia at day 12.

QUANTIFICATION AND STATISTICAL ANALYSIS

Differences in relative gRNA copies were tested with one-tailed T-tests on log-transformed data to meet normal distribution. Differences in gene expression and SM concentration were tested with multiple comparison LSD tests. A mixed-effects model with Geisser-Greenhouse correction was used to test differences in weight changes, clinical score and RNAemia in mice. Each group was compared to the control group using Dunnett's multiple comparisons test. Differences in survival were tested with Kaplan-Meier survival analysis with Log-rank (Mante-Cox) comparison test. The statistical analyses were performed using Prism 8.0.2 (GraphPad).